Transition from a meiotic to a somatic-like DNA damage response during the pachytene stage in mouse meiosis

Andrea Enguita-Marruedo[$], Marta Martín-Ruiz, Eva García, Ana Gil-Fernández, M. Teresa Parra, Alberto Viera, Julio S. Rufas and Jesus Page

Departamento de Biología, Facultad de Ciencias, Universidad Autónoma de Madrid, Madrid, Spain

[$]Current address: Department of Developmental Biology, Erasmus Medical Center, Rotterdam, The Netherlands

Correspondence to:

Jesus Page

e-mail: jesus.page@uam.es

Running tittle: Differential patterns of DNA repair in meiosis

Key Words: Meiosis, Homologous recombination, Non-homologous end joining, DMC1, RAD51, 53BP1, γH2AX, XRCC4.

Abstract

Homologous recombination (HR) is the principal mechanism of DNA repair acting during meiosis and is fundamental for the segregation of chromosomes and the increase of genetic diversity. Nevertheless, non-homologous end joining (NHEJ) mechanisms also act during meiosis, mainly in response to exogenously-induced DNA damage in late stages of first meiotic prophase. In order to better understand the relationship between these two repair pathways, we studied the response to DNA damage during male mouse meiosis after gamma radiation. We clearly discerned two types of responses immediately after treatment. From leptotene to early pachytene, exogenous damage triggered the massive presence of γH2AX throughout the nucleus, which was associated with DNA repair mediated by HR components (DMC1 and RAD51). This early pathway finished with the sequential removal of DMC1 and RAD51 and was no longer inducible at mid pachytene. However, from mid pachytene to diplotene, γH2AX appeared as large discrete foci. This late repair pattern was mediated first by NHEJ, involving Ku70/80 and XRCC4, which were constitutively present, and 53BP1, which appeared at sites of damage soon after irradiation. Nevertheless, 24 hours after irradiation, a HR pathway involving RAD51 but not DMC1 mostly replaced NHEJ. Additionally, we observed the occurrence of synaptonemal complex bridges between bivalents, most likely representing chromosome translocation events that may involve DMC1, RAD51 or 53BP1. Our results reinforce the idea that the early “meiotic” repair pathway that acts by default at the beginning of meiosis is replaced from mid pachytene onwards by a “somatic-like” repair pattern. This shift might be important to resolve DNA damage (either endogenous or exogenous) that could not be repaired by the early meiotic mechanisms, for instance those in the sex chromosomes, which lack a homologous chromosome to repair with. This transition represents another layer of functional changes that occur in meiotic cells during mid pachytene, in addition to epigenetic reprograming, reactivation of transcription, expression of a new gene profile and acquisition of competence to proceed to metaphase.

41 ## Author summary

42 DNA repair is critical for both somatic and meiotic cells. During meiosis, hundreds of DNA double strand
43 breaks (DSBs) are introduced endogenously. To repair this damage, meiotic cells use a specialized version
44 of the homologous recombination (HR) pathway that uses specific meiotic recombinases, such as DMC1,
45 to promote repair with the homologous chromosome instead of the sister chromatid. This process is
46 important to ensure chromosome segregation during meiosis and, as a side consequence, increases the
47 genetic diversity of offspring. Nevertheless, under specific circumstances, meiotic cells can use other DNA
48 repair mechanisms such as non-homologous end joining (NHEJ), which is error-prone. We investigated the
49 response of mouse spermatocytes to increased DNA damage caused by gamma radiation, which is
50 commonly used in cancer therapy. We found that the excess of DSBs produced by irradiation is processed
51 by the meiotic HR recombination pathway in spermatocytes at the early stages of first meiotic prophase.
52 However, this response is not inducible from the mid pachytene stage onwards. From this point on,
53 spermatocytes rely on a response that shares many features with that of somatic cells. In this response,
54 the NHEJ pathway is first used to repair DNA damage but is subsequently replaced by a HR mechanism
55 that does not use DMC1. Instead, it relies only on RAD51, which is known to function in both somatic and
56 meiosis cells and, contrary to DMC1, has a preference for the sister chromatid. This switch from a meiotic
57 to a somatic-like response is accompanied by a conspicuous change in the epigenetic response to DNA
58 damage, reinforcing the idea that a functional transition occurs in meiotic cells during the mid pachytene
59 stage.

60

Introduction

DNA damage response is one of the most critical processes for cell survival and proliferation. Of the different forms of DNA damage, double-strand breaks (DSBs) are by far the most harmful. DSBs can arise spontaneously as a consequence of exposure to physical and chemical agents or following replication errors. In somatic cells, two main mechanisms operate to repair DSBs [1]. Non-homologous end joining (NHEJ) is the most common mechanism, working in all phases of the cell cycle [2]. Although this pathway is quite efficient, it is also error-prone as it does not discriminate whether the two rejoined ends were the correct ones. In contrast, homologous recombination (HR) uses an intact DNA molecule as a template for repair, ensuring high fidelity of repair. However, this mechanism only acts when a DNA copy, usually the sister chromatid, is available, which only happens during the S/G_2 phases of the cell cycle.

During meiosis, homologous chromosomes undergo a series of complex processes, including pairing and synapsis, recombination and segregation. Meiotic recombination is in essence a HR DNA repair mechanism that ensures the proper segregation of chromosomes during the first meiotic division and increases genetic diversity [3,4]. Although the molecular mechanisms mediating HR in somatic and meiotic cells are similar, there are a number of differences, including the way DSBs are generated and some of the molecular components that work in their repair. In meiosis, HR begins after hundreds of DSBs are endogenously induced by Spo11 endonuclease during the leptotene stage of the first meiotic prophase [3,5,6]. The ATM kinase and the MRN protein complex (comprised of MRE11, RAD50 and NBS1) function as damage sensors by recognizing DSBs [7-9]. The MRN complex, together with other proteins (e.g. CtIP, BRCA1, BLM, EXO1, DNA2), then eliminates the covalent attachment of Spo11 and performs a 5' to 3' resection of DNA on either side of the break, which forms 3'-protruding ends of single-stranded DNA (ssDNA) [10]. The newly produced ssDNA is covered by RPA, which protects it from degradation [7]. Then,

the ATR-ATRIP (Ataxia Telangiectasia and Rad3-related and ATR-Interacting Protein) complex binds directly to the RPA-coated ssDNA, thus localizing the kinase ATR to DSBs [8].

After DNA resection, the recombinase proteins RAD51 and DMC1 replace RPA and form nucleoprotein filaments, allowing the ssDNA to invade the DNA double helix of the homologous chromosome [4,10]. Template choice for DSB repair is another specific feature of meiotic HR: it is tightly regulated to favor inter-homologue recombination and crossing-over, which ensure coordinated chromosomal disjunction at the first meiotic anaphase. DMC1, which is only expressed during meiosis, drives repair to favor non-sister chromatid donors, while RAD51, which is essential for both somatic and meiotic recombination, acts to favor sister-chromatid donors [6,11-13]. DNA contacts between homologous chromosomes can ultimately resolve as reciprocal or non-reciprocal recombination events, which lead to crossovers or gene conversion events, respectively.

Although HR is the main DNA repair pathway acting during meiosis, NHEJ can also be used [14]. The action of NHEJ mechanisms is apparently simpler. Classical NHEJ relies on the recruitment of the Ku70/80 complex and other regulatory factors, such as 53BP1, to the site of breaks to prevent DNA resection. This is followed by the incorporation of DNA-PKcs and DNA ligase IV, which reseals the break with the help of accessory factors such as XRCC4 [7,10]. In recent years, in addition to the classical NHEJ, a variety of alternative NHEJ pathways, which use additional biochemical components, have been uncovered [10,15]. Components of the classical NHEJ pathway such as Ku70/80 and 53BP1 have been detected in meiotic cells, both in the course of normal meiosis [16] and after the exogenous induction of DNA damage [14,17]. Not surprisingly, this mechanism seems to be triggered only in the late stages of first meiotic prophase. This may be a consequence of the upregulation of HR repair during the early stages of meiosis following the endogenous production of DSBs by Spo11 and the resection of DNA that is concomitant with Spo11 removal [18]. However, coexistence of HR and NHEJ is possible during the late

stages of meiotic prophase to repair DNA damage that was induced by either endogenous or exogenous mechanisms. Radiation exposure experiments, for instance, have reported an increase of both 53BP1 and RAD51 levels in pachytene and diplotene spermatocytes [14,17,19,20].

The key event for the choice between HR and NHEJ relies on the resection of DNA around the break [2]. The production of ssDNA overhangs hampers the action of NHEJ mechanisms, which require intact ends. Although the regulation of DNA resection at DSBs is not completely clear, a reciprocal regulation of factors promoting and inhibiting resection has been reported [21]. For instance, 53BP1 has been proposed to play a key role in inhibiting resection by hampering the loading of the CtIP-BRCA1 complex to the DNA, thus diverting repair to the NHEJ pathway [10,22,23]. CtIP-BRCA1, in turn, is thought to negatively regulate 53BP1 by inducing displacement of both 53BP1 and Ku70/80 from the break point and stimulating DNA resection by the MRN-(EXO1-DNA2-BLM) complex [2,24]. Interestingly, both 53BP1 and BRCA1 seem to rely on ATM kinase for phosphorylation, which is necessary for their function. Additional factors, such as the action of specific CDK-cyclin complexes and the epigenetic landscape around the break point also contribute to the regulation of DNA end resection [21].

In addition to the biochemical interactions described above, the morphological, temporal and epigenetic scenario in which DNA repair occurs during meiosis must be considered. Synapsis, the intimate association of homologues, is mediated by a highly specialized structure called the synaptonemal complex (SC) [25]. Assembly and disassembly of the SC during the first meiotic prophase is a tightly regulated process crucial for proper chromosome recombination and segregation [26], as evidenced by the number of synapsis mutants in which recombination is disturbed, and vice versa [27-31]. Furthermore, during first meiotic prophase, the complex regulation of transcription and chromatin modifications can influence the response to DNA damage [32-34]. Most conspicuously, histone H2AX is phosphorylated to give rise to γH2AX, which localizes throughout the nucleus during the leptotene stage in response to DSBs [35]. This

129 contrast with the pattern of γH2AX in somatic cells, where it usually forms small and discrete foci [36].
130 γH2AX is involved in recruiting many DNA repair factors [5,10,35,37,38] and in the transcriptional silencing
131 that characterizes the beginning of meiosis and sex chromosomes [33,35,39]. Notably, ATM, ATR and DNA-
132 PKcs can all phosphorylate H2AX [10,40,41]; therefore, γH2AX is a marker of both the HR and NHEJ
133 pathways. Upon DNA repair, γH2AX seems to be displaced from the chromatin and/or dephosphorylated
134 by protein phosphatases [42-44].

135 To shed light on the complex relationships of DNA repair mechanisms acting during meiosis, we
136 assessed DNA repair responses during mammalian male meiosis after the exogenous production of DSBs.
137 We irradiated mice with gamma rays and then analyzed the localization and dynamics of various markers
138 of DNA repair response, including γH2AX, DMC1, RAD51, 53BP1, Ku70 and XRCC4, at different times of
139 recovery. We have uncovered two distinct epigenetic patterns in response to DNA damage in early and
140 late prophase-I spermatocytes: a typical meiotic one and a somatic-like one acting at early and late stages,
141 respectively. The transition to a somatic-like response during mid pachytene coincides with the sequential
142 cessation of the meiotic HR response at mid pachytene and the consecutive activation of NHEJ and somatic
143 HR repair mechanisms. In addition, we report the formation of chromosome bridges between non-
144 homologous chromosomes associated with either HR or NHEJ markers.

145

Results

γH2AX dynamics after irradiation

We first analyzed the distribution pattern of γH2AX (H2AX phosphorylated at serine 139) in response to DNA damage. Phosphorylation of this histone is one of the first cytological events detected after DNA damage and has been used extensively to localize DSBs in both somatic and meiotic cells [5,10,35,36,38]. Staging of spermatocytes during first meiotic prophase was made on the basis of chromosome synapsis between autosomes and the morphology of the sex chromosomes following SYCP3 immunolabeling, as previously characterized [33].

In control spermatocytes, γH2AX is first detectable at early leptotene, when short threads of SYCP3 mark the initial assembly of axial elements (AEs) along the chromosomes. At this early stage, only a few discrete γH2AX foci are observed scattered throughout the nucleus (Fig 1A). During mid to late leptotene, when AEs form longer filaments, γH2AX is broadly localized throughout most of the nucleus (Fig 1B). This broad nuclear distribution is maintained during early zygotene (Fig 1C), when AEs start to synapse. From mid zygotene onwards, γH2AX signal decreases and, by the end of zygotene, is mainly associated with unsynapsed regions (Fig 1D). During pachytene, when homologous chromosomes are fully synapsed, γH2AX localizes almost exclusively on the sex chromosomes, which have extensive unsynapsed regions (Fig 1E and 2A-B). Nevertheless, large γH2AX foci are sometimes observed associated to the SCs of some autosomal bivalents. These foci have been previously described [5,33] and interpreted as unrepaired DSBs that tend to disappear with pachytene progression or, alternatively, as regions of transcriptional silencing [45]. During diplotene, when homologues desynapse, γH2AX remains present only on the sex chromosomes (Fig 2C).

In gamma-irradiated spermatocytes, visible changes in the pattern of γH2AX localization are observed one hour after irradiation. In early leptotene cells, γH2AX is seen throughout the nucleus, in contrast to the small scattered foci seen in controls, indicative of a massive broadly distributed DNA repair response (Fig 1F). This pattern is also observed in late leptotene, zygotene and early pachytene spermatocytes (Fig 1G-J). Changes at late leptotene and zygotene stages are less evident as γH2AX is already broadly localized throughout the nucleus in control cells at these stages. This pattern indicates that cells at the beginning of meiosis up to early pachytene respond to the induction of DNA damage similarly. In contrast, the response of spermatocytes from mid pachytene onwards is rather focalized. Large γH2AX foci are observed emerging from the SCs (Fig 2D-F). These kind of signals have been called large foci [5], flares [45] or eruptions [46]. The morphology of these foci resembles that found in control spermatocytes (Fig 2B) and somatic cells [36]. These results reveal the existence of morphological differences in the response to DNA damage between early and late meiotic prophase spermatocytes.

Irradiated spermatocytes show a clear diminution of γH2AX in most stages 24 hours after treatment. Similar to control cells, early leptotene cells have a few scattered γH2AX foci (Fig 1K). If we consider that meiotic progression is not greatly affected by irradiation, then cells should progress to further stages during the recovery time. Therefore, these early leptotene cells could have been at preleptotene when irradiated (see S1 Figure for an estimation of the length of each meiotic stage, based on previous reports [47,48]). In late leptotene and early-mid zygotene spermatocytes, γH2AX is distributed throughout the nucleus, similar to control cells (Fig 1L-M). Likewise, the pattern of γH2AX at late zygotene and early pachytene is comparable to that of the controls (Fig 1N-O), in which γH2AX appears to label the unsynapsed chromosomal regions and some foci in a few chromosomes. These cells were likely irradiated at leptotene and zygotene stages, respectively, indicating that cells irradiated at early meiotic stages are able to achieve a control pattern corresponding to their stage 24 hours after irradiation. Contrastingly, cells from mid pachytene to diplotene retain several foci associated with SCs (Fig 2G-I). These differences

191 are also observed 72 hours after irradiation (Fig 1P-T and 2J-L). In this case though, cells at mid pachytene
192 72 hours after irradiation were at an earlier pachytene stage at the time of irradiation. These cells likely
193 had widespread localization of γH2AX at an earlier stage in response to DNA damage but their γH2AX
194 pattern changes as they progress, very much like under endogenous production of DSBs. The persistence
195 of γH2AX foci, however, indicates incomplete DNA repair.

196 Notably, leptotene cells were very scarce 72 hours after irradiation. Previous reports indicated
197 that spermatogonia are particularly sensitive to radiation [17,19,49,50]. In order to confirm apoptosis of
198 these cells, we performed a TUNEL assay on testicular sections (S2 Fig) and observed an increase of
199 apoptosis in specific cell populations at different recovery times. Specifically, 24 hours post irradiation, a
200 noticeable, but not massive, increase of apoptosis is observed in spermatogonia and prophase-I
201 spermatocytes, while at 72 hours apoptosis is mainly observed in metaphase cells. This leads us to infer
202 that irradiation may partially ablate spermatogonia population, but probably also interrupts the normal
203 entrance of these cells in meiosis, which explains the scarcity of leptotene cells.

204 The two patterns of response to DSBs, early and late, also appear to differ in terms of γH2AX
205 removal. Spermatocytes irradiated at late pachytene or diplotene, or those that reach these stages during
206 recovery, remove γH2AX more slowly than those irradiated at earlier stages. In order to ascertain the
207 efficiency of DNA repair, we recorded the number of γH2AX foci from mid pachytene to diplotene (S3
208 Table) and analyzed the progression of repair by recovery time (Fig 2M) and cell stage (Fig 2N). One hour
209 after irradiation, the number of foci increases in the three stages. The ANOVA test showed no significant
210 differences between stages at this time. However, at 24 hours, the number of foci returns to control levels
211 in mid pachytene spermatocytes. In contrast, late pachytene and diplotene spermatocytes still show an
212 increased number of foci, which is maintained even 72 hours after treatment. These results support the

idea that γH2AX removal is less efficient as cells progress to later stages of prophase-I and that the number of foci seems to reach a steady state with no significant reduction.

Formation of chromosomal bridges

One striking feature observed after irradiation is the formation of connections between non-homologous chromosomes, which can be visualized by SYCP3 immunostaining (Fig 1T, 2J and 3). Connections are only occasionally observed in control individuals (although in some mouse strains, they appear more frequently; unpublished results). Connections are observed at all post-treatment times (1, 24 and 72 hours) and could be clearly identified in zygotene to diplotene spermatocytes. On the basis of their morphological appearance, we classified connections in three categories (Fig 3): 1) distal contacts, in which chromosomes interact end-to-end (Fig 3A-B); 2) interstitial contacts, in which a filament emerges from one bivalent and contacts one or more bivalents laterally (Fig 3C-F) and 3) intrachromosomal contacts, in which the connection is observed within the same bivalent (Fig 3G-I). In some cases, the SYCP3-positive filament of a bivalent seems to split into two with a thin filament, probably involving a single chromatid, providing the connection (Fig 3C). In other cases, the filament appears thicker (Fig 3D).

Chromosome connections can be observed between autosomal bivalents, between autosomes and sex chromosomes or between sex chromosomes. The presence of these bridges is likely not an artifact of the spreading technique as they are also observed in squashed spermatocytes (Fig 3J). Furthermore, chromosome fragments and bridges are observed during anaphase- and telophase-I (Fig 3K-L), indicating that these connections may represent chromosomal translocations. While connections between bivalents can result in a non-homologous chromosomal translocation, bridges within bivalents can potentially link the two homologous chromosomes or different parts of the same chromosome. The presence of these chromosomal aberrations at metaphase-I, which are rarely detected in the control cells, might account for the increased apoptosis observed at this stage 24 and 72 hours after treatment (S2 Fig).

In order to understand the dynamics of chromosome bridge formation, we quantified the number of cells showing at least one of these chromosomal connections during pachytene and diplotene (Fig 3M) (connections were more difficult to discern from chromosome tangles in earlier stages). No bridges were found in the controls. However, after irradiation, the frequency of spermatocytes bearing bridges increases from 6.48% at one hour to 9.15% at 24 hours and 24.13% at 72 hours, indicating a clear rise in the number of bridges with time. Regarding the distribution of bridges by stage and time, at 24 hours, most of the cells with bridges are at early pachytene; however, by 72 hours, the distribution is more uniform among stages.

Localization pattern of DMC1

In order to investigate the action of HR mechanisms, we first examined the spatial and temporal localization pattern of DMC1, which is exclusively present in meiosis and acts together with RAD51 [51,52]. To compare DMC1 distribution with the γH2AX pattern just described, we performed triple immunostaining of SYCP3, DMC1 and γH2AX. In control spermatocytes, DMC1 is first detected at the very beginning of leptotene, when AEs start to form along chromosomes. A few foci are seen scattered throughout the nucleus (Fig 4A), which are not specifically associated with either the short SYCP3 fragments or the small γH2AX foci already present. The presence of DMC1 foci at the beginning of leptotene suggested that they might be responding to DSBs produced by a SPO11-independent mechanism. However, their absence in SPO11 null mutants (S4 Fig) rules out this possibility. During late leptotene, many more DMC1 foci are clearly visible, and they appear to be mainly associated with chromosomal AEs (Fig 4B). During early zygotene, many DMC1 foci are still observed along both synapsed and unsynapsed chromosomal regions (Fig 4C). At late zygotene, the number of DMC1 foci decreases (Fig 4D). Some foci remain associated with autosomes but they are clearly more abundant on the unsynapsed AE of the X chromosome. A single DMC1 focus is observed on the Y chromosome. During early pachytene

(Fig 4E), even fewer foci are visible. Although DMC1 and γH2AX are co-localized on some autosomes, in many cases, DMC1 and γH2AX foci are not associated with one another (see detail in Fig 4E), indicating that DMC1 localization persists after the removal of γH2AX. At mid pachytene, most autosomal DMC1 foci have disappeared, though the sex chromosomes still have a high number of foci (Fig 4F). DMC1 is no longer detectable at a cytological level after mid pachytene.

After irradiation, a notable increase in DMC1 protein expression is observed (Fig 4G-Z), with foci associating with unsynapsed AEs during leptotene, synapsed and unsynapsed regions during zygotene and synapsed autosomes and the AE of the X chromosome from pachytene onwards. DMC1 is not detected beyond mid pachytene, indicating that this protein is not inducible by radiation exposure after this stage. Similar to control cells, some co-localization of DMC1 and γH2AX is observed in irradiated pachytene cells (see details in Fig 4K and 4L). We also observed DMC1-positive filaments connecting different chromosomes. These filaments are mainly present at 24 and 72 hours after irradiation and likely represent the nucleoprotein filaments formed during the ssDNA invasion of the intact DNA copy. Although it is unclear whether these filaments join homologous or heterologous chromosomes at earlier stages (Fig 4N), by pachytene, heterologous associations are clearly observed. Indeed, some of these filaments appear to be associated with SYCP3 threads that bridge different bivalents (Fig 4W-Z), indicating a role for DMC1 in DNA repair between heterologous chromosomes under experimental conditions.

Dynamics of DMC1 response

In order to analyze the dynamics of DNA repair associated with DMC1, we scored the number of foci in control and irradiated cells at different stages. On the basis of the morphological features of SC formation and the γH2AX localization pattern described above, we considered six different substages: early leptotene, mid-late leptotene, early-mid zygotene, late zygotene, early pachytene and mid pachytene. We

281 did not record the number of DMC1 foci in leptotene cells 72 hours post irradiation given the scarcity of
282 this cell population and the occurrence of morphological abnormalities, as mentioned above.

283 Our quantitative analysis revealed some interesting features (Fig 5 and S3 Table). First, the early
284 leptotene cell population of control spermatocytes has a low number of DMC1 foci and very low standard
285 deviation. As described above, this population is also characterized by a few small γH2AX foci. In contrast,
286 mid-late leptotene cells show an increase in the number and standard deviation of DMC1 foci, in
287 agreement with a previous report [53]. This stage is also associated with broad γH2AX labeling, as pointed
288 above. Peak abundance of DMC1 foci occurs during early-mid zygotene and decreases thereafter.
289 According to the ANOVA and Tukey's multiple comparisons tests, differences between each stage and the
290 next one are significant (Fig 5A), indicating that DMC1 distribution can be used to distinguish the cell
291 populations of the six substages.

292 Second, as expected, the number of foci increases one hour after irradiation in most phases (Fig
293 5). As in the control, peak abundance of DMC1 foci is observed in early-mid zygotene spermatocytes, and
294 each stage differs significantly from the following one, excepting mid-late leptotene and early-mid
295 zygotene. However, the number of DMC1 foci induced by irradiation differs greatly among the different
296 meiotic stages. The increase of foci compared to control is on average 69, 144, 76, 46, 18 and 4 for each
297 of the six substages, respectively (see S3 Table). This striking result indicates that the cell stages are not
298 equally sensitive to irradiation or that DMC1 localization to DSBs may be differentially regulated at the
299 different stages due to the availability of this protein or other DNA repair factors. Furthermore, in
300 irradiated mid pachytene spermatocytes, the number of DMC1 foci did not increase significantly regardless
301 of recovery time, indicating that DMC1 is no longer inducible at this or later stages. These results can be
302 more easily discerned when data are grouped by cell stage instead of recovery time (Fig 5B).

Third, after the increase of DMC1 foci immediately after irradiation, a slow diminution is observed with recovery time for most stages; however, most did not reach control levels even after 72 hours of recovery time (Fig 5B). Nevertheless, we observed two main stage-specific features. One, early leptotene cells show control levels 24 hours later. Moreover, while the number of DMC1 foci is quite variable one hour after treatment, 24 hours later, the range of foci narrows, very much like in the control. This finding may reflect the presence of newly formed leptotene cells that had just entered meiosis. Unfortunately, we could not record the number of DMC1 foci in early leptotene spermatocytes 72 hours after irradiation owing to the scarcity of this stage; and 2) in early pachytene, the number of DMC1 foci does not decrease but rather slightly increases with time. Assuming again that irradiation does not greatly disrupt meiotic progression, cells irradiated at a particular stage would continue to advance through meiosis and be at later stages when observed 24 or 72 hours later. Therefore, we arranged the quantitative data following a putative duration of 24 hours for leptotene, zygotene and early pachytene [34,47,50] (S1 and S5 Fig). This means that a cell irradiated at early leptotene would be at late leptotene-early zygotene 24 hours later and at early pachytene 72 hours later, and so on (S5 Fig). Considering four initial cell populations (early leptotene, late leptotene, early zygotene and late zygotene), we observed that, one hour after irradiation, the number of DMC1 foci increases in all cases and, in most cases, decreases 24 and 72 hours later, indicating efficient DNA repair in all cell populations. Nevertheless, control levels of DMC1 foci are not observed even after 72 hours of recovery, indicating that irradiation leads to an accumulation of DNA repair events. This contrasts with the quick and efficient removal of γH2AX at the same stages (Fig 1). The only exception are the cells that reach mid pachytene within the 72-hour period following irradiation. In this case, the levels of DMC1 did reach control levels, suggesting that DNA repair had been successfully completed in all cells. Alternatively, DMC1 might have been released from chromosomes at mid pachytene, regardless of whether repair had been completed or not.

Localization pattern and dynamics of RAD51

We then analyzed the distribution of RAD51, which acts with DMC1 in the HR pathway, in control and irradiated spermatocytes. In agreement with previous reports [51,52], we found that RAD1 has a similar, albeit not identical, distribution pattern as DMC1 during first meiotic prophase (Fig 6). During zygotene stage (Fig 6A, S6 and S7 Fig), RAD51 localizes to the AEs of chromosomes, with a peak number of foci observed mainly in early-mid zygotene, decreasing continuously thereafter. At early pachytene and later stages, RAD51 foci remain associated with some autosomal SCs but are mainly found on the unsynapsed AE of the X chromosome (Fig 6B and 6C). Most of these foci are not associated with γH2AX, which at this stage is restricted to a few foci. RAD51 disappears during late pachytene (Fig 6D) and is absent at diplotene (Fig 6E). This pattern is very similar to that of DMC1; however, we observed that RAD51 remains associated with chromosomes for a longer period of time, into later pachytene stages. In order to observe this more clearly, we performed double immunostaining for both proteins (S6 and S7 Fig). During early stages of prophase-I, the localization of both proteins is almost, but not completely, identical. We noticed that not all DMC1 foci are associated with RAD51 foci and vice versa and that foci morphology can differ. More importantly, these two proteins are removed from chromosomes sequentially since the number of RAD51 foci on both autosomes and sex chromosomes clearly exceeds that of DMC1 at the mid to late pachytene transition (S6E-E'' Fig). Thus, while the recruitment of RAD51 and DMC1 can be simultaneous upon the production of DSBs at the beginning of meiosis, persistent DSBs at the last stages of repair may lose DMC1 but maintain RAD51, which may reflect its role in promoting inter-sister versus inter-homolog interactions for the repair of DSBs [54].

Similar to the results with DMC1, we observed an increase in the number of RAD51 foci after irradiation (Fig 6F-T). Although we did not quantify the distribution of RAD51 at early meiotic stages, the broad co-localization of RAD51 and DMC1 up to mid pachytene (S6 and S7 Fig) suggests that both proteins follow a very similar pattern, i.e., peaking one hour after treatment then decreasing with recovery time.

However, the localization patterns of these proteins are not identical. For instance, though RAD51-positive filaments bridging chromosomes are also observed (S7 Fig), they are thinner and scarcer than DMC1 ones.

Strikingly, after irradiation, RAD51 is observed in late pachytene and diplotene spermatocytes (Fig 6I,J,N,O,S,T). Given that RAD51 is not observed at these stages in control spermatocytes, these foci must represent newly localized protein induced after irradiation. Indeed, this RAD51 population differs with the one observed at earlier stages. First, the signal strength of RAD51 on the sex chromosomes is similar to that of autosomes. Second, foci tend to be larger and sometimes irregularly shaped. Finally, while virtually all RAD51 foci observed at early stages (up to mid pachytene) are associated with the AEs or SCs, during late prophase, a significant proportion of RAD51 is detached from the SCs (Fig 6J,N,O). Most of these foci co-localize with γH2AX one hour after irradiation, indicating they correspond to regions of DNA damage (Fig 6J and 6O).

To examine the dynamics of this late-appearing population of RAD51, we scored the number of foci present in mid pachytene to late diplotene spermatocytes (Fig 7A and 7B; S3 Table). This analysis uncovered some interesting features. First, one hour after irradiation, RAD51 increases significantly in all stages analyzed except mid pachytene. This striking result parallels the behavior of DMC1, which is also not inducible at mid pachytene, suggesting that HR repair can be compromised at this stage immediately after irradiation. The increase of RAD51 in late prophase spermatocytes is modest but significant, with no statistical differences observed among late pachytene and early and late diplotene stages. Second, after 24 hours of recovery, the number of RAD51 foci is significantly higher in all cell populations, though the increase is more pronounced in late pachytene cells and conspicuously lower in diplotene cells. After 72 hours of recovery, RAD51 levels remain high, though a slight decrease is observed in all stages, except mid pachytene. No statistical differences are detected between early and late diplotene, except in the number of foci at 24 hours. This difference could be caused by a small fraction of cells passing from late pachytene

373 into early diplotene during this period, resulting in a higher number of RAD51 foci in early diplotene
374 spermatocytes. The unexpected behavior of RAD51 during mid-late pachytene and diplotene stages
375 suggests that the HR response to induction of exogenous DSBs initially may be absent or weak but
376 increases with time, at least until 24 hours after irradiation.

377 We were intrigued by the presence of RAD51 foci that were not associated with SCs. We analyzed
378 the dynamics of RAD51 foci during diplotene (Fig 7C and S3 Table) and found that both SC-associated and
379 non-associated RAD51 foci follow the same pattern, increasing one hour after irradiation, peaking 24 hours
380 later and decreasing thereafter. We found that the number of foci associated with SCs is clearly higher in
381 cells at early and late diplotene but that the proportion of non-associated RAD51 foci increases in late
382 diplotene cells 24 and 72 hours after irradiation.

383 **Localization of NHEJ markers**

384 In order to ascertain the action of the NHEJ repair mechanism, we studied the temporal and spatial
385 localization of different components of this pathway. We first examined the localization of Ku70, which is
386 involved in the protection of broken DNA ends, and XRCC4, which is a ligase-IV co-factor. Immunostaining
387 of these proteins yielded nearly identical results; therefore, we will only show the localization of XRCC4
388 (Fig 8). Neither protein is observed during early meiotic stages in control spermatocytes (Fig 8A). At late
389 pachytene, however, a weak signal appears throughout the nucleus (Fig 8B) and becomes more intense at
390 diplotene (Fig 8C). At this stage, the signal appears slightly more intense over the sex chromosomes. In
391 order to rule out the absence of XRCC4 labeling in early spermatocytes as an artifact of the spreading
392 technique, we also immunostained testicular sections (S8 Fig). XRCC4 is absent in the basal spermatocytes
393 of the seminiferous tubules and is only detectable in spermatocytes located in the middle of the
394 epithelium, corresponding to late pachytene-diplotene cells. These results indicate that these components
395 are present by default during the normal course of meiosis, in agreement with previous reports [14,16].

We observed a very similar pattern in irradiated spermatocytes: no signal is detected prior to late pachytene and, from this stage onwards, the proteins are distributed homogeneously throughout the nucleus (Fig 8D-L; S8 Fig). Although we did not quantify fluorescence intensity, no marked differences in the signal strengths of these proteins were observed between control and irradiated cells. Moreover, neither Ku70 nor XRCC4 accumulates at putative DSB sites after irradiation (e.g. in a pattern resembling that of γH2AX). Therefore, induction of DNA damage has little to no effect on the spatial and temporal localization of Ku70 and XRCC4, consistent with these proteins being present by default at these stages.

We also analyzed the localization of 53BP1, which has a main role in protecting broken DNA ends from resection during NHEJ repair. In control cells, 53BP1 is absent during leptotene, zygotene and early pachytene (not shown) but present by mid pachytene (Fig 9A), accumulating over the chromatin of the sex chromosomes in the same space occupied by γH2AX. 53BP1 signal is maintained during late pachytene (Fig 9B) and early diplotene (Fig 9C) but becomes weak by late diplotene. Occasionally, a weak signal is found on some autosomes.

After irradiation, in addition to sex chromosomes, 53BP1 localizes to the autosomes from mid pachytene up to the end of diplotene. One hour after treatment (Fig 9D-F), a large number of irregularly shaped foci are observed on the autosomes, very similar to the γH2AX eruptions. Indeed, most 53BP1 foci on the autosomes co-localize with γH2AX, although unassociated foci of both proteins are also observed. The same pattern is found at both 24 (Fig. 9G-I) and 72 hours after treatment (Fig 9J-L). We observed that some chromosomal bridges, which are frequent in cells after treatment, are associated with 53BP1 (Fig 10J), indicating the involvement of NHEJ repair pathway proteins in this type of chromosome interaction.

The quantitative analysis of 53BP1 after treatment (Fig 9M-N, S3 Table) shows the dramatic increase in the number of foci one hour after irradiation in mid- and late pachytene and early diplotene spermatocytes and its sharp decline 24 and 72 hours later. This pattern clearly contrasts with and seems

419 antagonistic to that of RAD51, with NHEJ proteins acting as a fast response and HR proteins acting in two
420 phases, weakly immediately after DNA damage and strongly 24 hours later. We also observed that late
421 stages tend to have more 53BP1 foci, indicating stage-specific differences in the response. Nevertheless,
422 by 72 hours after irradiation, all stages show control levels of 53BP1.

423

Discussion

The accurate repair of DNA damage is critical for the survival of cells. Meiosis is an excellent model to investigate the response of cells to genomic damage owing to the occurrence of programmed DNA DSBs. However, the response to this endogenous damage must coexist with the sporadic occurrences of exogenous DNA damage, for instance, that caused by exposure to ionizing radiation. The specific processes that occur during meiosis, with the assembly of the SC being the most relevant, work in combination with the endogenous program to bias DSB repair towards the HR pathway [14,16]. Nevertheless, at the end of first meiotic prophase, some constraints might be relaxed, allowing the operation of somatic-like mechanisms. The results presented here offer new ways to understand the interplay of these two responses including how and when this transition occurs during meiosis.

Different stages of prophase I have different responses to DNA damage

Phosphorylation of histone H2AX is one of the first key events to occur in response to DNA damage. As shown here and in previous reports, one hour after exposure to gamma radiation, γH2AX levels increase during all stages of first meiotic prophase [20]. However, two types of responses can be clearly distinguished according to the cellular phase: a massive response, characterizing the early stages, in which γH2AX marks the entire nucleus, and a more focused response from mid pachytene to diplotene in which γH2AX instead localizes as large and well-defined foci. This focused response is typically found in somatic cells [36] even though, under irradiation overexposure, both somatic and meiotic cells can show a pan-nuclear response [20,55]. However, in our case, all cells were exposed to the same dose of irradiation; therefore, the differences in response are not due to dosage-dependent effects. The origin of these differences could be related, in part, to changes in chromatin configuration and transcriptional activity, as previously suggested for somatic cells [56]. Highly dynamic replacement and modification of histones and proteins associated with chromatin are known to occur during prophase-I [33,34,57-59]. Mouse

447 spermatocytes in early prophase-I are characterized by a widespread distribution of histone H3
448 monomethylated at lysine 4 and trimethylated at lysine 9, which are both related to chromatin compaction
449 and transcriptional repression [33,34,60]. These modifications are lost or re-localized between early and
450 mid pachytene, concomitant with other relevant epigenetic changes, such as the incorporation of histone
451 H1t, which is related to the competency of cells to proceed to chromatin condensation stages [57], and a
452 general reactivation of transcriptional activity, which is accompanied by the acetylation of histone H3 and
453 other associated factors [33,34,61,62]. Therefore, the epigenetic changes occurring in meiotic cells at this
454 stage likely act as regulatory factors modulating the DNA damage response.

455 Changes in chromosome organization may also play a role in the shift in the DNA damage
456 response. In *C. elegans*, changes in both chromatin conformation and organization of the SC central
457 element are proposed to be involved in the change in the DNA damage response during the mid to late
458 pachytene transition [63,64]. Indeed, exogenous damage can lead to desynapsis of homologous
459 chromosomes [64]. Although no dramatic remodeling of the SC occurs in mouse spermatocytes during this
460 transition, the gradual shortening of the SC during pachytene, which results in longer chromatin loops, is
461 a feature that potentially resembles such reorganization and thus may change the framework in which
462 DNA repair proteins function.

463 An additional cause of this change may be related to the different kinases that promote H2AX
464 phosphorylation. At least two rounds of H2AX phosphorylation dependent on two different kinases have
465 been proposed to occur in mouse meiosis: the first during leptotene involving ATM and the second at the
466 end of zygotene involving ATR [39,46]. Our efforts to corroborate this hypothesis by immunostaining for
467 kinases, including ATM, ATR and DNA-PK, were unsuccessful. However, indirect proof can be inferred. In
468 this sense, ATM kinase activity seems to produce an amplification loop in the phosphorylation of H2AX
469 that extends up to several megabases beyond the DSBs [41], whereas the phosphorylation produced by

ATR and DNA-PKcs entails a more focused response in which the signal is limited to areas close to DSBs [65]. Therefore, the two responses we observed with γH2AX may reflect a main role of ATM at the beginning of prophase-I and a higher activity of ATR and DNA-PKcs at later stages [46]. Interestingly, the response of somatic cells to irradiation, in which most DSBs are repaired by NHEJ [66,67], usually produces discrete foci of γH2AX in the nucleus [36,41], similar to those found in pachytene and diplotene spermatocytes. Therefore, it seems that early stages have a meiotic-specific γH2AX response, while late stages have a repair response more similar to somatic cells (Fig 10).

Based on γH2AX removal, the early response seems to be more efficient as cells irradiated at early stages return to control levels 24 after treatment. In contrast, cells irradiated at later meiotic stages retain a number of γH2AX foci for the duration of recovery. This contradicts findings that, on the basis of the removal dynamics of several repair proteins, suggested repair of DSBs induced at early stages of meiosis is slower than those occurring at later stages [19]. Therefore, it is important to be cautious with these interpretations. We found that many of the γH2AX foci observed at the different stages and recovery times are not associated with DMC1, RAD51 or 53BP1. The persistence of γH2AX in late stages may not be completely related to a delay in the completion of DNA repair but instead to delayed dephosphorylation or turnover of the histone [36]. A similar persistence of γH2AX foci has been also reported after etoposide-induced damage [20]. On the other hand, a substantial number of DMC1, RAD51 or 53BP1 foci are associated with chromosomes long after γH2AX has been displaced. Indeed, the number of DMC1/RAD51 foci in in cells irradiated at early stages is still above control levels 72 hours after irradiation (except in mid pachytene cells); this also applies for RAD51 and 53BP1 foci in late pachytene and diplotene cells, indicating the persistence of unrepaired events. Therefore, it seems that the production of exogenous DSBs challenges both early and late repair pathways during meiosis, resulting in an overall lower efficiency of meiotic repair of exogenous damage compared to somatic cells, as has been previously suggested [17,19].

Response to endogenous DNA damage involves similar, but not identical, responses of DMC1 and RAD51

Our analysis of DSB repair pathways clearly indicates that HR is preeminent or exclusive at early meiotic stages, up to mid pachytene, and reveals interesting clues about the pattern of HR response under both normal and experimental situations.

In relation to the initiation of damage response in leptotene under normal conditions, we identified a population of early leptotene cells that is characterized by a low number of γH2AX and DMC1/RAD51 foci. Then, a burst of these proteins is detected in late leptotene. Although we cannot rule out the possibility that these two patterns are just the two extremes of a linear rise of DSBs during leptotene [53], it is also possible that they represent two different physiological stages. While early DSBs are clearly SPO11-dependent, the rate in which they arise is limited, probably owing to the action of a limited number of SPO11 complexes [53,68] or to restrictions imposed by associated factors. Some proteins that stimulate Spo11 activity, like IHO1, are associated with the AEs [69]. Therefore, DSB production could be limited in a chromosomal context in which AEs have not yet formed. Given this context, these DSBs would be able to only trigger a focus-limited (somatic-like?) γH2AX response. The extensive γH2AX labeling of this early leptotene population after irradiation indicates that these cells are competent to display a broad (meiotic) γH2AX reaction. Nonetheless, this *bona fide* meiotic response is only detected later in leptotene, once AEs have become more extended. This interpretation poses interesting questions about the transition from spermatogonia to meiosis, which includes other puzzling features like the premeiotic pairing of homologous chromosomes [70].

An intriguing issue arose when we compared the distribution of DMC1 and RAD51. We noticed that these two proteins tend to form mixed foci but that their localization patterns are not identical. Several studies reporting similar findings in budding yeast, plants and female mouse meiosis have

517 suggested that these proteins occupy different positions along the nucleoprotein filaments [54,71,72],
518 perhaps performing complementary functions. More strikingly, we found that the temporal pattern of
519 DMC1 and RAD51 do not coincide, particularly in the transition from mid to late pachytene. DMC1
520 disappears from both autosomes and sex chromosomes at this stage, leaving only RAD51 on
521 chromosomes. Temporal displacement between DMC1 and RAD51 loading and unloading has been also
522 observed in plant meiosis [73]. This result may provide insight on the last stages of meiotic DNA repair
523 pattern, particularly on the sex chromosomes. Several studies have hypothesized that DSBs on the X and
524 Y chromosomes do not have homologous templates which can be used for repair, except obviously the
525 pseudoautosomal region, and that repair can only be accomplished with the sister chromatid
526 [32,35,74,75]. DMC1 may play a key role in interhomolog bias [54], such that its persistence on the sex
527 chromosomes may explain why unresolved DSBs remain on these chromosomes long after most breaks
528 have been repaired on the autosomes. The removal of DMC1 from sex chromosomes, and autosomes, at
529 the mid-late pachytene stage may relax interhomolog bias, allowing RAD51 to then drive repair with the
530 sister chromatid.

531 **Response to irradiation in early meiosis is characterized by the action of HR proteins that end**
532 **at mid pachytene**

533 Irradiation clearly stimulates the increase in the number of DMC1 and RAD51 foci from early leptotene up
534 to early pachytene. We did not find any markers for NHEJ at these stages. Although we cannot rule out
535 that alternative NHEJ pathways independent of Ku70 or 53BP1 might be present, it seems that the early
536 response is mostly mediated by HR mechanisms, consistent with the findings of other studies [16,17,19].
537 It is reasonable to assume that induction of additional breaks will simply use machinery that is already
538 present. Therefore, endogenous and exogenous DSBs can enter the same repair pathway. Consequences
539 of this include, for instance, an increased number of chiasmata, as previously reported [19,76].

Nevertheless, this response is limited as prophase-I proceeds. The net increase of DMC1/RAD51 foci at each stage is lower as spermatocytes move to more advanced stages. Most strikingly, a meiotic HR response to exogenous DNA damage is very weak or not detected at mid pachytene, thus providing additional evidence of the functional shift of spermatocytes at this stage (Fig 10). This transition likely involves the cessation of expression of some meiotic-specific genes (like DMC1) and the initiation of a new gene expression profile [77-79]. This is interesting not only in terms of DNA repair but also in relation to the regulation of meiotic progression. Several studies have provided evidence of a pachytene checkpoint that monitors DNA repair, chromosome synapsis and other physiological processes such as sex chromosome inactivation [39,47,80-82]. Although the mechanisms that drive this checkpoint in mouse have not been completely elucidated, defective spermatocytes appear to be largely eliminated at a specific point of meiotic progression, identified as stage IV of the seminiferous epithelium in mouse, which most likely corresponds to the mid pachytene stage [47,80,83]. Once cells have cleared this checkpoint, inactivation of these surveillance mechanisms would be necessary to allow the progression of spermatocytes to later stages, allowing for instance desynapsis of chromosomes during diplotene without triggering meiotic progression arrest or inactivation of desynapsing regions. Likewise, inactivation of the early meiotic DNA damage response would be necessary after passing the checkpoint at mid pachytene, with new events of DNA damage that occur from this stage onwards being subject to new control mechanisms, as previously suggested [20]. These new mechanisms would rely on different checkpoints, as exemplified by the elimination of spermatocytes in mutant mice for late recombination proteins such as MLH1 or MLH3 at metaphase-I [84,85].

NHEJ response is quickly stimulated upon irradiation from mid pachytene onwards

One may expect that, in the absence of a DMC1 response at mid pachytene, RAD51 takes the role of driving HR repair at this stage. As discussed above, RAD51 remains associated with chromosomes after DMC1 has

563 detached, and previous reports have indicated that RAD51 is inducible in late prophase-I after irradiation
564 treatments [17,19,20]. Consistent with this, one hour after irradiation, we found a modest but clear
565 increase in RAD51 from late pachytene onwards; however, the increase was not significant at mid
566 pachytene. Instead, we observed increased levels of 53BP1 at all stages from mid pachytene to late
567 diplotene, indicating a faster response of the NHEJ pathway at these stages. Although RAD51 levels are
568 increased in irradiated late pachytene and diplotene spermatocytes compared to controls, the number of
569 53BP1 foci clearly exceeds that of RAD51. This contrasts with a previous study that reported the presence
570 of 53BP1 only after longer periods of recovery [17]. Differences in methodological approaches used to
571 determine 53BP1 localization might account for these discrepancies.

572 The quick trigger of NHEJ in late prophase-I may be due to a change in the choice of the default
573 mechanism for DSB repair (Fig 10). Somatic cells first attempt to use NHEJ to repair DSBs, even in the G_2
574 phase of the cell cycle when a sister chromatid is available to carry out more reliable repair by HR [2,15,86].
575 The choice of NHEJ as the default mechanism from late pachytene onwards is illustrated by the constitutive
576 presence of Ku70 and XRCC4 in the nucleus and the location of 53BP1 on the sex chromosomes. Therefore,
577 as soon as new exogenous or even endogenous DNA breaks appear, this mechanism would quickly
578 respond. This makes complete sense in terms of the biochemistry of DNA repair. Given that the choice
579 between NHEJ or HR relies on the regulation of DNA resection around the break point [10], for which
580 53BP1 has an inhibitory role [22,23], it is clear that NHEJ must be a first option. Otherwise, once resection
581 has been performed, repair by this mechanism would be no longer possible. Nevertheless, it also clear that
582 both mechanisms are acting at the same time, raising the possibility that NHEJ and HR proteins are
583 competing for DNA repair, especially from late pachytene onwards. In any case, after 24 hours of recovery,
584 few 53BP1 loci remain, which may be due to rapid repair by NHEJ [2], but also to competition with HR. In
585 somatic cells, HR seems to be preeminent in regions of high transcriptional activity [56], which is indeed

586 the case of late pachytene and diplotene cells during meiosis. In any case, the increased presence of RAD51
587 foci 24 hours after irradiation indicates that HR repair mechanisms prevail again at that time.

588 **Late HR response involves RAD51 only**

589 The late HR response has many differences with the early one. The most relevant is that it only involves
590 RAD51. In the transition to a somatic-like DNA damage response, DMC1 is clearly no longer inducible, likely
591 related to the change in gene expression pattern during pachytene [77-79]. The activity of RAD51 alone
592 means that some of the constraints introduced by DMC1 in relation to DNA repair, such as homologous
593 bias [6,11,12,54], would be relaxed. Therefore, this late repair could favor repair with the sister chromatid,
594 which would be advantageous at the diplotene stage as desynapsis of chromosomes potentially hinders
595 repair with the homologous chromosome.

596 The RAD51 foci present during the late HR response are larger. Although we do not have a clear
597 explanation for the morphological change of RAD51 foci, differential organization of the repair machinery
598 around the break point involving, for instance, the accumulation of several DSBs in each foci, or comprising
599 the resection of longer DNA stretches, may account for this change, as previously suggested in *C. elegans*
600 [63]. These foci are also correlated with the formation of smaller discrete γH2AX foci, which, as mentioned
601 above, may be due to the action of ATR or DNA-PK over ATM in the phosphorylation of H2AX, leading to a
602 different architecture of the repair foci [41,65].

603 Finally, the finding of RAD51 foci not associated with the AEs/SCs of chromosomes is an intriguing
604 feature. Whether RAD51 foci are always associated with AEs/SCs has been a matter of long debate [87].
605 Current models propose that endogenous DSBs in early stages are produced either in the context of the
606 AE or rapidly taken there by the action of regulatory factors, including MEI4, IHO1 and HORMAD1, among
607 others [69,88]. This is probably provided by their ability to interact with SPO11 before or at the time of
608 DSB production. We found that most DSBs induced after radiation also localize at the AEs/SCs, as revealed

by the pattern of DMC1/RAD51 foci and as reported in a previous study [50]. Thus, at early meiotic stages, both endogenous and exogenously induced DSBs likely rely on similar mechanisms to be taken to the chromosomal axis. However, at late stages, the situation might be different. The presence of IHO1 and HORMAD1 has been reported in diplotene cells [69,89]; however, it remains unclear whether these proteins, or others required for DSB localization at the axes, are completely functional at these stages. Partial failure of this process might explain the fraction of DSBs located far from AEs/SCs. Likewise, the progressive loss of these proteins as prophase-I proceeds may account for the increased frequency of non-associated foci in late diplotene spermatocytes compared with previous stages.

Homologous recombination homeostasis and chromosomal bridges

The appearance of chromosomal bridges involving SYCP3-positive filaments is an intriguing feature that poses a number of questions about the nature of DNA repair. The presence of chromosomal connections and fragments is commonly found in irradiation experiments [90,91]; however, they are usually observed in metaphase and do not involve SC connections. To our knowledge, our study is the first to report that interactions between non-homologous chromosomes may involve not only the DNA contacts but also the axial structures they are attached to. This contrasts with the normal interactions of endogenous DSBs, which do not involve the formation of connections between the AEs of homologous chromosomes. A more in-depth characterization of these connections is needed to better understand the organization of the SC around break points and their role in promoting, facilitating or stabilizing chromosomal links.

Bridges appear soon after irradiation, indicating they are part of a very fast response, and at increased frequencies with recovery times. Moreover, although we cannot rule out that some bridges are present at leptotene (see Fig. 4N), they are undoubtedly present at all stages from zygotene to diplotene. In fact, according to our quantitative analysis, bridges are more frequent in early pachytene spermatocytes

and less frequent in later phases. Several possible interpretations can be drawn from these results. Given that bridges are observed between non-homologous chromosomes, or between non-homologous sequences of the same chromosome (intrachromosomal junctions), one would expect that they correspond to DSBs repaired by NHEJ. However, the appearance of bridges at early stages such as zygotene and early pachytene, in which the main repair mechanism is HR, challenges this interpretation. Our immunostainings of Ku70, XRCC4 and 53BP1 indicate that NHEJ does not operate at early stages; however, alternative NHEJ mechanisms may potentially be present. Involvement of the NHEJ repair pathway in the formation of chromosomal bridges is doubtless only from mid pachytene onwards.

The presence of chromosomal bridges at early stages may be a consequence of the action of the HR pathway over homologous regions. This idea may seem completely counterintuitive but would be supported by the observation of DMC1/RAD51 filaments bridging non-homologous chromosomes. For HR to efficiently start, a minimum length of perfect homology is needed, which in mammals is 200-250 base pairs [10]. For this reason, repair templates are usually the sister chromatid or the homologous chromosome. However, the multitude of repeated sequences in the genome could provide sufficient homology to induce repair by HR. In the normal course of meiosis, endogenous DSBs are prevented over repeated DNA sequences. Moreover, mismatch repair mechanisms are in place to avoid recombination between highly homologous sequences of non-homologous chromosomes [92]. In addition, the number of DSBs is tightly regulated to not exceed a certain number, thus allowing mismatch repair mechanisms to function effectively [93]. Proteins like MEI4 and IHO1 seem to be involved in this limitation [69,88]. However, the excess of DSBs produced by radiation may have a deregulatory effect on the control of repair mechanisms such that homology requirements may be bypassed, thus allowing repair between non-homologous chromosomes.

654 Regardless of the mechanisms used to form bridges, the final output is the production of
655 chromosome connections that likely lead to the occurrence of translocations and fragmentation. This may
656 cause cells to be compromised in the faithful distribution of chromosomes during the first meiotic division.
657 Indeed, a noticeable increase of apoptosis is observed in metaphase/anaphase cells 24 and 72 hours after
658 irradiation.

659

Conclusions

The results presented here provide new insights on the transition between different programs of DNA repair during meiosis that act in a stage-dependent manner. A switch in DNA damage repair responses during meiosis has been also reported in other animal models such as *C. elegans* [63,64] and *Drosophila* [94]. Strikingly, these transitions also occur at the mid or late pachytene stages, indicating they may represent a conserved feature of meiosis. However, since both *Drosophila* and *C. elegans* control synapsis and DNA repair differently than mammals, particularly as they lack a DMC1 orthologue, the regulation of this transition might be different.

The evidence presented also offers new clues about the location and dynamics of DNA repair mechanisms during meiosis and raises new questions about the differential functions performed by DMC1 and RAD51. The late HR pathway very much resembles the somatic response, presenting focalized γH2AX and involving only RAD51. This somatic-like response likely acts to repair DSBs that were not properly repaired by the meiotic default pathway (e.g. those on the sex chromosomes) or the occasional DNA damage that occurs after the primary phase of meiotic repair has concluded until cells start to condense chromatin and prepare for cell division. At this point, re-triggering a complex repair mechanism leading to the production of crossovers (provided chiasmata formation has been properly accomplished) would not be necessary. A simpler response using NHEJ or somatic HR would be sufficient. As previously suggested [63], this shift could simply be contributing to the maintenance of genome integrity before spermatocytes are engaged in segregating chromosomes to daughter cells.

Materials and methods

Adult CD1 male mice were used in this study. Animals were kept at the animal facility of the Universidad Autonoma de Madrid, following the animal care standards of the institution. All experiments were approved by the UAM Ethics Committee (certificate CEI 55-999-A045). Males were exposed to 5Gy gamma radiation in a CIS Bio International irradiator, equipped with a Cesium^{137} source. Mice were sacrificed by cervical dislocation 1, 24 and 72 hours after irradiation and the seminiferous tubules processed as described below. Testicular samples of SPO11 knockout mice [31] were kindly shared by Dan Camerini-Otero (NIDDK, NIH, Bethesda, MD).

Cell spreads and squashes

For spermatocyte spreads, we used the procedure described by Peters and coworkers [95]. Seminiferous tubules were disaggregated with forceps in a petri dish and a cell suspension was collected in phosphate buffered saline (PBS: 137 mM NaCl, 2.7 mM KCl, 10.1 mM Na2HPO4, 1.7 mM KH2PO4, pH 7.4). After tubule fragments settled to the bottom of the dish, the cell suspension was transferred to a tube and centrifuged. The pellet was then resuspended in 400 µl of 100 mM sucrose. Cells were spread onto a slide submerged in 1% formaldehyde in distilled water containing 50 mM Na2B4O7 and 0.15% Triton X-100 and then left to dry for two hours. Slides were subsequently washed with 0.04% Photo-Flo (Kodak) in distilled water and air-dried before being used for immunofluorescence or stored at -80°C.

Spermatocyte squashes were prepared as previously described [96]. Seminiferous tubules were fixed for 10 minutes in 2% formaldehyde in PBS containing 0.1 % Triton X-100. Fragments of tubules were placed on a slide coated with 1 mg/ml poly-L-lysine (Sigma) with two drops of fixative. A coverslip was put on top of the tubules and the cells were released by gently pressing the coverslip with a pencil. Finally,

tubules were squashed, the slide was frozen in liquid nitrogen and the coverslip removed with a blade. Slides were immediately placed in PBS for further use.

Immunofluorescence

Spread and squashed slides were rinsed three times for 5 min each in PBS and incubated overnight at room temperature with primary antibodies diluted in PBS. The following primary antibodies and dilutions were used: mouse monoclonal anti-SYCP3 (Abcam, 97672) at 1:200; rabbit anti-SYCP3 (Abcam, 15093) at 1:100; mouse monoclonal against histone H2AX phosphorylated at serine 139 (γ-H2AX) (Upstate, 05-636) at 1:1000; rabbit anti-DMC1 (Santa Cruz, SC-22768) at 1:50; rabbit anti-RAD51 (Santa Cruz SC-8349) at 1:50; rabbit anti-53BP1 (Abcam 36823) at 1:100; goat anti-XRCC4 (Santa Cruz, SC-8285) at 1:100; goat anti-Ku70 (Santa Cruz, SC-1486) at 1:50. After incubation, slides were rinsed in PBS three times for 5 minutes each and subsequently incubated with the appropriate secondary antibodies in a moist chamber at room temperature for 1 h. We used anti-rabbit, anti-mouse and anti-goat secondary antibodies raised in donkey and conjugated with either Alexa 350, Alexa 488, Alexa 594 (Invitrogen), DyLight 549 or DyLight 649 (Jackson ImmunoResearch). Slides were subsequently rinsed in PBS three times for 5 min each and mounted with Vectashield (Vector). For double detection of two antibodies raised in the same species, we used Fab secondary antibodies as previously described [97].

Observations were made on an Olympus BX61 microscope equipped with a motorized Z axis. Images were captured with an Olympus DP72 digital camera using the Cell-F software (Olympus, Hamburg, Germany) and processed using the public domain software ImageJ (National Institutes of Health, USA; http://rsb.info.nih.gov/ij) and Adobe Photoshop 7.0.

Testicular sections and TUNEL assay

722 Testicles were fixed in cold 1% formaldehyde in PBS for 6 hours and then dehydrated and embedded in
723 paraffin. Transverse sections (7 µm) were cut and mounted onto slides. Slides were then deparaffinized
724 and treated with 0.1% sodium citrate buffer containing 0.1% Triton-X 100 for 10 min at 37°C. Sections were
725 subsequently processed for immunofluorescence as described above or for TUNEL (Roche) following
726 manufacturer instructions. Slides were counterstained with DAPI and mounted with Vectashield.

727 **Statistical analysis**

728 γ-H2AX, DMC1, RAD51 and 53BP1 foci and chromosomal bridges were scored manually and the
729 results were compared between different cell stages and times after irradiation. At least 25 cells were
730 scored for each protein, treatment and cell stage. For the TUNEL assay, 300 tubules were analyzed for
731 each treatment, recording the proportion of tubules with apoptotic cells and the total number of positive
732 cells, which were classified as spermatogonia, prophase-I and division spermatocytes owing to their size,
733 position on the seminiferous epithelium and chromosome condensation. Data were analyzed using
734 ANOVA and Tukey's multiple comparison tests for individual comparisons between different stages.
735 Statistics and graphics were made using GraphPad Prism 6 or Excel software.

736

Acknowledgements

We are grateful to Dr. Dan Camerini-Otero for generously sharing samples of SPO11 knockout mice and to Dr. Monica Pradillo and Willy Baarends for their critical review of the manuscript.

References

1. Ceccaldi R, Rondinelli B, D'Andrea AD (2016) Repair Pathway Choices and Consequences at the Double-Strand Break. Trends in cell biology 26: 52-64.
2. Shibata A (2017) Regulation of repair pathway choice at two-ended DNA double-strand breaks. Mutation Research/Fundamental and Molecular Mechanisms of Mutagenesis.
3. Ehmsen KT, Heyer WD (2008) Biochemistry of Meiotic Recombination: Formation, Processing, and Resolution of Recombination Intermediates. Genome Dyn Stab 3: 91.
4. Krejci L, Altmannova V, Spirek M, Zhao X (2012) Homologous recombination and its regulation. Nucleic Acids Res 40: 5795-5818.
5. Chicheportiche A, Bernardino-Sgherri J, de Massy B, Dutrillaux B (2007) Characterization of Spo11-dependent and independent phospho-H2AX foci during meiotic prophase I in the male mouse. J Cell Sci 120: 1733-1742.
6. Neale MJ, Keeney S (2006) Clarifying the mechanics of DNA strand exchange in meiotic recombination. Nature 442: 153-158.
7. Langerak P, Russell P (2011) Regulatory networks integrating cell cycle control with DNA damage checkpoints and double-strand break repair. Philos Trans R Soc Lond B Biol Sci 366: 3562-3571.
8. Shiotani B, Zou L (2009) ATR signaling at a glance. J Cell Sci 122: 301-304.
9. Andersen SL, Sekelsky J (2010) Meiotic versus mitotic recombination: two different routes for double-strand break repair: the different functions of meiotic versus mitotic DSB repair are reflected in different pathway usage and different outcomes. Bioessays 32: 1058-1066.
10. Grabarz A, Barascu A, Guirouilh-Barbat J, Lopez BS (2012) Initiation of DNA double strand break repair: signaling and single-stranded resection dictate the choice between homologous recombination, non-homologous end-joining and alternative end-joining. Am J Cancer Res 2: 249-268.
11. La Volpe A, Barchi M (2012) Meiotic double strand breaks repair in sexually reproducing eukaryotes: we are not all equal. Exp Cell Res 318: 1333-1339.
12. Schwacha A, Kleckner N (1997) Interhomolog Bias during Meiotic Recombination: Meiotic Functions Promote a Highly Differentiated Interhomolog-Only Pathway. Cell 90: 1123-1135.
13. Cloud V, Chan Y-L, Grubb J, Budke B, Bishop DK (2012) Rad51 Is an Accessory Factor for Dmc1-Mediated Joint Molecule Formation During Meiosis. Science 337: 1222-1225.
14. Ahmed EA, Philippens ME, Kal HB, de Rooij DG, de Boer P (2010) Genetic probing of homologous recombination and non-homologous end joining during meiotic prophase in irradiated mouse spermatocytes. Mutat Res 688: 12-18.
15. Her J, Bunting SF (2018) How cells ensure correct repair of DNA double-strand breaks. Journal of Biological Chemistry.
16. Goedecke W, Eijpe M, Offenberg HH, van Aalderen M, Heyting C (1999) Mre11 and Ku70 interact in somatic cells, but are differentially expressed in early meiosis. Nat Genet 23: 194-198.
17. Ahmed EA, van der Vaart A, Barten A, Kal HB, Chen J, et al. (2007) Differences in DNA double strand breaks repair in male germ cell types: lessons learned from a differential expression of Mdc1 and 53BP1. DNA Repair (Amst) 6: 1243-1254.
18. Neale MJ, Pan J, Keeney S (2005) Endonucleolytic processing of covalent protein-linked DNA double-strand breaks. Nature 436: 1053-1057.
19. Schoenmakers S, Wassenaar E, van Cappellen WA, Derijck AA, de Boer P, et al. (2008) Increased frequency of asynapsis and associated meiotic silencing of heterologous chromatin in the presence of irradiation-induced extra DNA double strand breaks. Dev Biol 317: 270-281.
20. Matulis S, Handel MA (2006) Spermatocyte responses in vitro to induced DNA damage. Molecular Reproduction and Development 73: 1061-1072.

788 21. Daley JM, Niu H, Miller AS, Sung P (2015) Biochemical mechanism of DSB end resection and its
789 regulation. DNA Repair 32: 66-74.
790 22. Bunting SF, Callen E, Wong N, Chen HT, Polato F, et al. (2010) 53BP1 inhibits homologous
791 recombination in Brca1-deficient cells by blocking resection of DNA breaks. Cell 141: 243-254.
792 23. Panier S, Boulton SJ (2014) Double-strand break repair: 53BP1 comes into focus. Nat Rev Mol Cell Biol
793 15: 7-18.
794 24. Guirouilh-Barbat J, Gelot C, Xie A, Dardillac E, Scully R, et al. (2016) 53BP1 Protects against CtIP-
795 Dependent Capture of Ectopic Chromosomal Sequences at the Junction of Distant Double-Strand
796 Breaks. PLoS Genet 12: e1006230.
797 25. Page SL, Hawley RS (2004) The genetics and molecular biology of the synaptonemal complex. Annual
798 Review of Cell and Developmental Biology 20: 525-558.
799 26. Cahoon CK, Hawley RS (2016) Regulating the construction and demolition of the synaptonemal
800 complex. Nat Struct Mol Biol 23: 369-377.
801 27. de Vries FA, de Boer E, van den Bosch M, Baarends WM, Ooms M, et al. (2005) Mouse Sycp1 functions
802 in synaptonemal complex assembly, meiotic recombination, and XY body formation. Genes Dev
803 19: 1376-1389.
804 28. Yuan L, Liu JG, Zhao J, Brundell E, Daneholt B, et al. (2000) The murine SCP3 gene is required for
805 synaptonemal complex assembly, chromosome synapsis, and male fertility. Mol Cell 5: 73-83.
806 29. Revenkova E, Eijpe M, Heyting C, Hodges CA, Hunt PA, et al. (2004) Cohesin SMC1 beta is required for
807 meiotic chromosome dynamics, sister chromatid cohesion and DNA recombination. Nat Cell Biol
808 6: 555-562.
809 30. Baudat F, Manova K, Yuen JP, Jasin M, Keeney S (2000) Chromosome synapsis defects and sexually
810 dimorphic meiotic progression in mice lacking Spo11. Mol Cell 6: 989-998.
811 31. Romanienko PJ, Camerini-Otero RD (2000) The mouse Spo11 gene is required for meiotic chromosome
812 synapsis. Mol Cell 6: 975-987.
813 32. Inagaki A, Schoenmakers S, Baarends WM (2010) DNA double strand break repair, chromosome
814 synapsis and transcriptional silencing in meiosis. Epigenetics 5: 255-266.
815 33. Page J, de la Fuente R, Manterola M, Parra MT, Viera A, et al. (2012) Inactivation or non-reactivation:
816 what accounts better for the silence of sex chromosomes during mammalian male meiosis?
817 Chromosoma 121: 307-326.
818 34. van der Heijden GW, Derijck AA, Posfai E, Giele M, Pelczar P, et al. (2007) Chromosome-wide
819 nucleosome replacement and H3.3 incorporation during mammalian meiotic sex chromosome
820 inactivation. Nat Genet 39: 251-258.
821 35. Mahadevaiah SK, Turner JM, Baudat F, Rogakou EP, de Boer P, et al. (2001) Recombinational DNA
822 double-strand breaks in mice precede synapsis. Nat Genet 27: 271-276.
823 36. Rothkamm K, Barnard S, Moquet J, Ellender M, Rana Z, et al. (2015) DNA damage foci: Meaning and
824 significance. Environmental and Molecular Mutagenesis 56: 491-504.
825 37. Hamer G, Roepers-Gajadien HL, van Duyn-Goedhart A, Gademan IS, Kal HB, et al. (2003) DNA double-
826 strand breaks and gamma-H2AX signaling in the testis. Biol Reprod 68: 628-634.
827 38. Banerjee T, Chakravarti D (2011) A peek into the complex realm of histone phosphorylation. Mol Cell
828 Biol 31: 4858-4873.
829 39. Turner JM, Mahadevaiah SK, Fernandez-Capetillo O, Nussenzweig A, Xu X, et al. (2005) Silencing of
830 unsynapsed meiotic chromosomes in the mouse. Nat Genet 37: 41-47.
831 40. Durocher D, Jackson SP (2001) DNA-PK, ATM and ATR as sensors of DNA damage: variations on a
832 theme? Curr Opin Cell Biol 13: 225-231.
833 41. Yuan J, Adamski R, Chen J (2010) Focus on histone variant H2AX: to be or not to be. FEBS Lett 584:
834 3717-3724.

42. Chowdhury D, Keogh MC, Ishii H, Peterson CL, Buratowski S, et al. (2005) gamma-H2AX dephosphorylation by protein phosphatase 2A facilitates DNA double-strand break repair. Mol Cell 20: 801-809.
43. Kinner A, Wu W, Staudt C, Iliakis G (2008) Gamma-H2AX in recognition and signaling of DNA double-strand breaks in the context of chromatin. Nucleic Acids Res 36: 5678-5694.
44. Svetlova MP, Solovjeva LV, Tomilin NV (2010) Mechanism of elimination of phosphorylated histone H2AX from chromatin after repair of DNA double-strand breaks. Mutation Research/Fundamental and Molecular Mechanisms of Mutagenesis 685: 54-60.
45. Moens PB, Marcon E, Shore JS, Kochakpour N, Spyropoulos B (2007) Initiation and resolution of interhomolog connections: crossover and non-crossover sites along mouse synaptonemal complexes. Journal of Cell Science 120: 1017-1027.
46. Bellani MA, Romanienko PJ, Cairatti DA, Camerini-Otero RD (2005) SPO11 is required for sex-body formation, and Spo11 heterozygosity rescues the prophase arrest of Atm-/- spermatocytes. J Cell Sci 118: 3233-3245.
47. Ashley T, Gaeth AP, Creemers LB, Hack AM, de Rooij DG (2004) Correlation of meiotic events in testis sections and microspreads of mouse spermatocytes relative to the mid-pachytene checkpoint. Chromosoma 113: 126-136.
48. Oakberg EF (1956) Duration of spermatogenesis in the mouse and timing of stages of the cycle of the seminiferous epithelium. Am J Anat 99: 507-516.
49. van der Meer Y, Huiskamp R, xe, Jan AGD, van der Tweel I, et al. (1992) The Sensitivity of Quiescent and Proliferating Mouse Spermatogonial Stem Cells to X Irradiation. Radiation Research 130: 289-295.
50. Carofiglio F, Sleddens-Linkels E, Wassenaar E, Inagaki A, van Cappellen WA, et al. (2018) Repair of exogenous DNA double-strand breaks promotes chromosome synapsis in SPO11-mutant mouse meiocytes, and is altered in the absence of HORMAD1. DNA Repair (Amst) 63: 25-38.
51. Plug AW, Peters AH, Keegan KS, Hoekstra MF, de Boer P, et al. (1998) Changes in protein composition of meiotic nodules during mammalian meiosis. J Cell Sci 111 (Pt 4): 413-423.
52. Tarsounas M, Morita T, Pearlman RE, Moens PB (1999) RAD51 and DMC1 form mixed complexes associated with mouse meiotic chromosome cores and synaptonemal complexes. J Cell Biol 147: 207-220.
53. Cole F, Kauppi L, Lange J, Roig I, Wang R, et al. (2012) Homeostatic control of recombination is implemented progressively in mouse meiosis. Nature cell biology 14: 424-430.
54. Brown MS, Bishop DK (2015) DNA Strand Exchange and RecA Homologs in Meiosis. Cold Spring Harbor Perspectives in Biology 7.
55. Meyer B, Voss K-O, Tobias F, Jakob B, Durante M, et al. (2013) Clustered DNA damage induces pan-nuclear H2AX phosphorylation mediated by ATM and DNA–PK. Nucleic Acids Res 41: 6109-6118.
56. Aymard F, Bugler B, Schmidt CK, Guillou E, Caron P, et al. (2014) Transcriptionally active chromatin recruits homologous recombination at DNA double-strand breaks. Nature Structural &Amp; Molecular Biology 21: 366.
57. Cobb J, Cargile B, Handel MA (1999) Acquisition of Competence to Condense Metaphase I Chromosomes during Spermatogenesis. Dev Biol 205: 49-64.
58. Handel MA (2004) The XY body: a specialized meiotic chromatin domain. Exp Cell Res 296: 57-63.
59. Hoyer-Fender S (2003) Molecular aspects of XY body formation. Cytogenet Genome Res 103: 245-255.
60. van Dijk K, Marley KE, Jeong B-r, Xu J, Hesson J, et al. (2005) Monomethyl Histone H3 Lysine 4 as an Epigenetic Mark for Silenced Euchromatin in Chlamydomonas. The Plant Cell Online 17: 2439-2453.
61. Burgoyne PS, Mahadevaiah SK, Turner JM (2009) The consequences of asynapsis for mammalian meiosis. Nat Rev Genet 10: 207-216.

62. Monesi V (1965) Synthetic activities during spermatogenesis in the mouse RNA and protein. Exp Cell Res 39: 197-224.
63. Hayashi M, Chin GM, Villeneuve AM (2007) C. elegans Germ Cells Switch between Distinct Modes of Double-Strand Break Repair During Meiotic Prophase Progression. PLoS Genet 3: e191.
64. Couteau F, Zetka M (2011) DNA Damage during Meiosis Induces Chromatin Remodeling and Synaptonemal Complex Disassembly. Developmental Cell 20: 353-363.
65. Scully R, Xie A (2013) Double strand break repair functions of histone H2AX. Mutat Res.
66. Fattah F, Lee EH, Weisensel N, Wang Y, Lichter N, et al. (2010) Ku regulates the non-homologous end joining pathway choice of DNA double-strand break repair in human somatic cells. PLoS Genet 6: e1000855.
67. Rogakou EP, Boon C, Redon C, Bonner WM (1999) Megabase chromatin domains involved in DNA double-strand breaks in vivo. J Cell Biol 146: 905-916.
68. Lange J, Pan J, Cole F, Thelen MP, Jasin M, et al. (2011) ATM controls meiotic double-strand-break formation. Nature 479: 237-240.
69. Stanzione M, Baumann M, Papanikos F, Dereli I, Lange J, et al. (2016) Meiotic DNA break formation requires the unsynapsed chromosome axis-binding protein IHO1 (CCDC36) in mice. Nature cell biology 18: 1208-1220.
70. Boateng Kingsley A, Bellani Marina A, Gregoretti Ivan V, Pratto F, Camerini-Otero RD (2013) Homologous Pairing Preceding SPO11-Mediated Double-Strand Breaks in Mice. Developmental Cell 24: 196-205.
71. Kurzbauer M-T, Uanschou C, Chen D, Schlögelhofer P (2012) The Recombinases DMC1 and RAD51 Are Functionally and Spatially Separated during Meiosis in Arabidopsis. The Plant Cell 24: 2058-2070.
72. Carofiglio F, Inagaki A, de Vries S, Wassenaar E, Schoenmakers S, et al. (2013) SPO11-Independent DNA Repair Foci and Their Role in Meiotic Silencing. PLoS Genet 9: e1003538.
73. Sanchez-Moran E, Santos J-L, Jones GH, Franklin FCH (2007) ASY1 mediates AtDMC1-dependent interhomolog recombination during meiosis in Arabidopsis. Genes & Development 21: 2220-2233.
74. Kauppi L, Jasin M, Keeney S (2012) The tricky path to recombining X and Y chromosomes in meiosis. Ann N Y Acad Sci 1267: 18-23.
75. Ashley T, Plug AW, Xu J, Solari AJ, Reddy G, et al. (1995) Dynamic changes in Rad51 distribution on chromatin during meiosis in male and female vertebrates. Chromosoma 104: 19-28.
76. Cai X, Li J, Yang Q, Shi Q (2011) Gamma-irradiation increased meiotic crossovers in mouse spermatocytes. Mutagenesis 26: 721-727.
77. Shima JE, McLean DJ, McCarrey JR, Griswold MD (2004) The murine testicular transcriptome: characterizing gene expression in the testis during the progression of spermatogenesis. Biol Reprod 71: 319-330.
78. da Cruz I, Rodríguez-Casuriaga R, Santiñaque FF, Farías J, Curti G, et al. (2016) Transcriptome analysis of highly purified mouse spermatogenic cell populations: gene expression signatures switch from meiotic-to postmeiotic-related processes at pachytene stage. BMC Genomics 17: 294.
79. Margolin G, Khil PP, Kim J, Bellani MA, Camerini-Otero RD (2014) Integrated transcriptome analysis of mouse spermatogenesis. BMC Genomics 15: 39.
80. Barchi M, Mahadevaiah S, Di Giacomo M, Baudat F, de Rooij DG, et al. (2005) Surveillance of different recombination defects in mouse spermatocytes yields distinct responses despite elimination at an identical developmental stage. Mol Cell Biol 25: 7203-7215.
81. Roeder GS, Bailis JM (2000) The pachytene checkpoint. Trends Genet 16: 395-403.
82. Roig I, Dowdle JA, Toth A, de Rooij DG, Jasin M, et al. (2010) Mouse TRIP13/PCH2 Is Required for Recombination and Normal Higher-Order Chromosome Structure during Meiosis. PLoS Genetics 6: e1001062.

931 83. de Rooij DG, de Boer P (2003) Specific arrests of spermatogenesis in genetically modified and mutant
932 mice. Cytogenet Genome Res 103: 267-276.
933 84. Lipkin SM, Moens PB, Wang V, Lenzi M, Shanmugarajah D, et al. (2002) Meiotic arrest and aneuploidy
934 in MLH3-deficient mice. Nature Genetics 31: 385.
935 85. Baker SM, Plug AW, Prolla TA, Bronner CE, Harris AC, et al. (1996) Involvement of mouse Mlh1 in DNA
936 mismatch repair and meiotic crossing over. Nature Genetics 13: 336.
937 86. Mansour WY, Schumacher S, Rosskopf R, Rhein T, Schmidt-Petersen F, et al. (2008) Hierarchy of
938 nonhomologous end-joining, single-strand annealing and gene conversion at site-directed DNA
939 double-strand breaks. Nucleic Acids Res 36: 4088-4098.
940 87. Moens PB, Chen DJ, Shen Z, Kolas N, Tarsounas M, et al. (1997) Rad51 immunocytology in rat and
941 mouse spermatocytes and oocytes. Chromosoma 106: 207-215.
942 88. Kumar R, Ghyselinck N, Ishiguro Ki, Watanabe Y, Kouznetsova A, et al. (2015) MEI4 – a central player
943 in the regulation of meiotic DNA double-strand break formation in the mouse. Journal of Cell
944 Science 128: 1800-1811.
945 89. Wojtasz L, Daniel K, Roig I, Bolcun-Filas E, Xu H, et al. (2009) Mouse HORMAD1 and HORMAD2, Two
946 Conserved Meiotic Chromosomal Proteins, Are Depleted from Synapsed Chromosome Axes with
947 the Help of TRIP13 AAA-ATPase. PLoS Genet 5: e1000702.
948 90. Calvente A, Santos JL, Rufas JS (2016) Do Exogenous DNA Double-Strand Breaks Change Incomplete
949 Synapsis and Chiasma Localization in the Grasshopper Stethophyma grossum? PLOS ONE 11:
950 e0168499.
951 91. Matsuda Y, Ohara H, Tobari I (1987) Studies on radiation-induced chromosome aberrations in mouse
952 spermatocytes II. Dose-response relationships of chromosome aberrations induced at zygotene
953 stage in mouse primary spermatocytes following fast neutron- and 60Co γ-irradiations. Mutation
954 Research/Fundamental and Molecular Mechanisms of Mutagenesis 176: 251-257.
955 92. Spies M, Fishel R (2015) Mismatch Repair during Homologous and Homeologous Recombination. Cold
956 Spring Harbor Perspectives in Biology 7.
957 93. Keeney S, Lange J, Mohibullah N (2014) Self-Organization of Meiotic Recombination Initiation: General
958 Principles and Molecular Pathways. Annual Review of Genetics 48: 187-214.
959 94. Mehrotra S, McKim KS (2006) Temporal analysis of meiotic DNA double-strand break formation and
960 repair in Drosophila females. PLoS Genet 2: e200.
961 95. Peters AH, Plug AW, van Vugt MJ, de Boer P (1997) A drying-down technique for the spreading of
962 mammalian meiocytes from the male and female germline. Chromosome Res 5: 66-68.
963 96. Page J, Suja JA, Santos JL, Rufas JS (1998) Squash procedure for protein immunolocalization in meiotic
964 cells. Chromosome Res 6: 639-642.
965 97. Page J, Berrios S, Rufas JS, Parra MT, Suja JA, et al. (2003) The pairing of X and Y chromosomes during
966 meiotic prophase in the marsupial species Thylamys elegans is maintained by a dense plate
967 developed from their axial elements. J Cell Sci 116: 551-560.

968

969

970

971 # Figure legends

972 **Figure 1. Pattern of γH2AX after irradiation in early prophase mouse spermatocytes.** SYCP3 (green) and
973 γH2AX (blue) at different stages of prophase I by recovery time after irradiation. (A-E) Control. (A) Early
974 leptotene. γH2AX localizes as small scattered foci over the short threads of forming AEs. (B) Mid-late
975 leptotene. AEs are more extended and now a massive γH2AX signal covers the nucleus. This pattern is also
976 found in early zygotene (C), when AEs are completely formed and homologues start to synapse. (D) Late
977 zygotene. Homologous chromosomes have nearly completed synapsis. γH2AX signal still occupies large
978 chromatin regions, mostly on the unsynapsed autosomes and the X chromosome (X). The Y chromosome
979 (Y) is usually devoid of massive γH2AX labeling. (E). Early pachytene. Autosomes are completely synapsed,
980 whereas sex chromosomes show a variable degree of synapsis. γH2AX extends over both sex
981 chromosomes (X and Y) and regions of chromatin around some autosomes (arrows). (F-J) 1 hour of
982 recovery. Increased γH2AX signal is observed in the nucleus of spermatocytes from early leptotene to early
983 pachytene. The signal covers the entire nucleus at all the stages, contrasting with the pattern of control
984 cells. (K-O) 24 hours of recovery. There is an evident decrease in the amount of γH2AX in early leptotene,
985 late zygotene and early pachytene spermatocytes, comparable to the controls. γH2AX localizes around the
986 sex chromosomes, and some foci present in autosomes (arrows). (P-T) 72 hours of recovery. A pattern
987 analogous to that at 24 hours is found. Chromosomal connections involving SYCP3 are observed between
988 some bivalents (arrowhead).

989

990 **Figure 2. Pattern of γH2AX after irradiation in late prophase mouse spermatocytes.** SYCP3 (green) and
991 γH2AX (blue) at different stages of prophase-I by recovery time after irradiation. (A-C) Control. γH2AX
992 appears around the sex chromosomes (X and Y) in mid pachytene (A), late pachytene (B) and diplotene
993 (C). Occasionally, some small foci remain associated with autosomes (arrowheads). (D-F). 1 hour of

994 recovery. In addition to the sex chromosomes, γH2AX localizes on the autosomes as large foci that emerge
995 from the SCs (arrowheads) at all three stages. (G-I). 24 hours of recovery. All stages show a visible decrease
996 in the amount of γH2AX. In mid pachytene cells (G), γH2AX foci are almost absent yet many foci are still
997 present in late pachytene (H) and diplotene (I) cells. (J-L). 72 hours of recovery. The pattern is similar to 24
998 hours; some foci (arrowheads) remain present in late pachytene (K) and diplotene (L) cells. Some
999 chromosomal connections are visible and appear to involve γH2AX signals (arrows). (M) Dotplot of the
1000 number of γH2AX foci in spermatocytes grouped by recovery time. The increase in the number of foci is
1001 evident 1 hour after irradiation. ANOVA analysis showed no statistical differences at this time between
1002 the three stages analyzed ($p=0.22$). Tukey's multiple comparisons test for individual comparisons between
1003 different stages showed no statistical differences. 24 hours after irradiation, a reduction in the number of
1004 foci is observed at all stages, but now statistical differences between stages are observed (ANOVA
1005 $p\leq0.0001$). Individual comparisons indicate the existence of differences between all stages. An analogous
1006 situation is found 72 hours after irradiation (ANOVA $p\leq0.0001$). (N) Dotplot of the number of γH2AX foci
1007 in spermatocytes grouped by stage. While mid pachytene cells return to levels similar to the control 24
1008 hours after irradiation ($p\geq0.05$), late pachytene and diplotene do not at any time after irradiation. MP: mid
1009 pachytene; LP: late pachytene; D: diplotene; ns: non-significant; *: $p\leq0.05$; **: $p\leq0.01$; ***: $p\leq0.001$; ****:
1010 $p\leq0.0001$.

1011

1012 **Figure 3. Types of chromosomal bridges.** SYCP3 protein in green. (A-I) Spread spermatocytes at pachytene,
1013 except (G), which is at zygotene. (A) Distal junction between two autosomes. (B) Distal junction between
1014 an autosome and a sex chromosome, in this case the X. (C-D) Interstitial junctions between autosomal
1015 bivalents. In (C) a bivalent with two bridges, each contacting a different bivalent, is shown. In the inset, a
1016 higher power view of one of the bridges is shown. The lateral element of the homologue involved in the

bridge is split into two filaments. One filament remains associated with the homologous chromosome and the other is linked to the chromosome of the other bivalent. In (D) two bivalents are sharing a bridge. In this case, the bridge is a whole counterpart, which has invaded the other bivalent. A higher power view of the bridge is shown in the inset. (E) Interstitial junctions between an autosomal bivalent and the X chromosome. In (F) a bridge is formed between an autosomal bivalent and the Y chromosome. (G) Chromosomal bridge within an autosomal bivalent. (H) Chromosomal bridge within the X chromosome. (I) Chromosomal bridge within the Y chromosome. (J-L) Squashed spermatocytes. DNA was counterstained with DAPI and false colored in red. (J) Bridges are seen in 3-dimension conserved cells. During anaphase-I (K) and telophase-I (L), chromosomal fragments and connections (arrows) are observed. (M). Graph showing the frequency of cells showing at least one bridge at the different cell stages of prophase-I and at the different time points after irradiation. The number of cells with bridges increases with recovery time. Chromosomal connections are especially represented in early pachytene cells. n = total number of cells analyzed.

Figure 4. Pattern of DMC1 at different stages of prophase-I by recovery time after irradiation. SYCP3 (red), γH2AX (blue) and DMC1 (green). (A-F) Control. (A) Early leptotene. A few small foci of DMC1 appear distributed throughout the nucleus; however, they do not seem to specifically co-localize with SYCP3 or γH2AX. (B) Mid-late leptotene. DMC1 foci are more abundant and now mostly associated with short SYCP3 filaments. (C). Early-mid zygotene. DMC1 foci are very abundant over the formed AEs, some of which are undergoing synapsis. (D). Late zygotene. DMC1 foci are located over both synapsed and unsynapsed chromosomes. Some signal co-localizes with remaining clouds of γH2AX, while others do not. The X chromosome (X) appears coated with many foci, while only a single focus is seen on the Y chromosome (Y). Gradually, DMC1 foci disappear during early pachytene (E) and mid pachytene (F), but remain on the

sex chromosomes and some autosomes. Only occasionally do some of these DMC1 foci co-localize with γH2AX (see detail in E). (G-L) 1 hour of recovery. The number of DMC1 foci increases at all stages from leptotene to early pachytene. At early leptotene (G), DMC1 coincides with the increase and spread of γH2AX to the whole nucleus. The number of DMC1 foci is clearly higher than in the control shown in A. No conspicuous differences in the pattern of DMC1 are observed at late leptotene (H) or zygotene (I-J). The Y chromosome still shows a single DMC1 focus. In early (K) and mid pachytene (L) spermatocytes, DMC1 is observed on autosomes and sex chromosomes. Again, DMC1 foci may co-localize or not with γH2AX. Enlarged views of some bivalents (arrows) are shown as insets in panels K and L. Chromosomal bridges are also found (arrowheads). (M-R) 24 hours of recovery. The distribution of γH2AX resembles that of control cells at all stages but the number of DMC1 foci seems reduced compared with cells 1 hour after irradiation. In some cells DMC1 appears to form filaments, sometimes joining AEs together (see arrowheads and detail in N). (S-Z). 72 hours of recovery. Leptotene cells (S-T) are found at a very low frequency and usually include morphological distortions. The morphological features of cells from zygotene to mid pachytene are similar to those found at 24 hours. Again, small DMC1 filaments appear on the chromosomes. These filaments seem to occasionally mediate the formation of bridges between two bivalents (arrowheads and details in W and Z); in some cases, γH2AX signal is associated with bridges (Z).

Figure 5. Dotplot representation of DMC1 foci distribution. (A) Analysis of DMC1 distribution by time of recovery. Six substages were considered (EL: early leptotene; LL: mid-late leptotene; EZ: early-mid zygotene; LZ: late zygotene; EP: early pachytene; MP: mid pachytene). The six populations, including early leptotene, are clearly distinguishable in the control. A low number of foci is found in EL cells but numbers increase in LL, peak in EZ and then gradually decrease in LZ, EP and MP cells. ANOVA analysis showed statistical differences ($p \leq 0.0001$) for the control and the three recovery times, and Tukey's multiple

comparisons test for individual comparisons between different stages showed statistical differences in all cases, except between LL and EZ 1 hour after irradiation (ns: non-significant; *: p≤0.05; **: p≤0.01; ***: p≤0.001; ****: p≤0.0001). (B) Analysis of DMC1 distribution by cell stage. ANOVA analysis showed that the number of DMC1 foci increased at all stages after irradiation (p≤0.0001) except mid pachytene (p=0.89). The increase of DMC1 foci observed 1 hour after irradiation compared to control is lower as cells are in more advances stages, and no increase is found at mid pachytene. Likewise, differences in the number of foci between 1 and 24 hours, or between 24 and 72 hours, become less or not significant as cells are in later stages. Nevertheless, control levels in terms of number of foci were not observed for any of the stages, even after 72 hours of recovery, except obviously mid pachytene. Tukey's multiple comparisons test for individual comparisons (ns: non-significant; *: p≤0.05; **: p≤0.01; ***: p≤0.001; ****: p≤0.0001).

Figure 6. Pattern of RAD51 at different stages of prophase-I by different recovery time after irradiation. SYCP3 (red), γH2AX (blue) and RAD51 (green). (A-F) Control. (A) Late Zygotene. RAD51 foci are found in the non-synaptic AEs, which are also labeled with γH2AX, some synapsed autosomes and the sex chromosomes (X and Y). During early (B) and mid (C) pachytene, fewer RAD51 foci are observed. Some remain on the autosomes, but most are in the non-synapsed region of the X chromosome. RAD51 does not appear during the late pachytene (D) and diplotene (E). (F-J) 1 hour of recovery. Irradiation induces RAD51 in zygotene (F) and early pachytene (H) spermatocytes. RAD51 can still be detected in late pachytene (I) and diplotene (J) spermatocytes. Most RAD51 foci are located over the AEs or SCs (white arrows). Insets show enlarged views of RAD51 foci co-localizing with γH2AX (white arrowheads), RAD51 foci alone (green arrowheads) and γH2AXfoci alone (blue arrowheads). Some RAD51 foci are clearly detached from the AEs or SCs (green arrows in J). (K-O) 24 hours of recovery. RAD51 coincides with γH2AX during zygotene (K), while at later stages (L-O), co-localization of the two signals does not always occur

(see detail in N). In late pachytene (N) and diplotene (O) spermatocytes, RAD51 foci are more abundant than at 1 hour. Foci are also larger. Green arrows indicate RAD51 foci not associated with SCs. (P-T) 72 hours of recovery. The pattern is similar to the results obtained after 24 hours of recovery. Most RAD51 foci are large and coincide with γH2AX during late pachytene (S) and diplotene (T).

Figure 7. Dotplot representation of RAD51 foci distribution. (A) Analysis of RAD51 distribution by recovery time. Four substages were considered (MP: mid pachytene; LP: late pachytene; ED: early diplotene; LD: late diplotene). ANOVA analysis showed statistical differences ($p \leq 0.0001$) for the control and the three recovery times. In the control, MP cells have a high number of RAD51 foci but later-staged cells have little to none. A similar increase in the number of RAD51 foci is observed from LP to LD 1 hour after irradiation. Tukey's multiple comparisons test for individual comparisons showed statistical differences between MP and the rest of the stages, and also between LP and LD. Twenty-four hour after irradiation, the increase in the number of RAD51 is more obvious at all stages, while 72 hours after irradiation, the number of foci decreases from LP to LD. (B) Analysis of RAD51 distribution by cell stage. The number of RAD51 foci increases significantly in cells at all stages after irradiation ($p \leq 0.0001$). However, according to Tukey's test, the number of foci in irradiated mid pachytene cells 1 hour after irradiation is not significantly different from control cells. At 24 hours, the number of foci increases in mid pachytene cells and remains stable at 72 hours. This distribution departs from the pattern observed in cells at other stages, in which RAD51 increases slightly at 1 hour, peaks at 24 hours and then decreases at 72 hours. (ns: non-significant; *: $p \leq 0.05$; **: $p \leq 0.01$; ***: $p \leq 0.001$; ****: $p \leq 0.0001$). (C). Analysis of RAD51 foci associated (ON) or not associated (OFF) with SCs at early and late diplotene. The distribution of both kinds of foci is similar, increasing at 1 hour, peaking at 24 hours and decreasing at 72 hours. Notably, the proportion of foci not associated with SCs (OFF) is higher in late diplotene spermatocytes.

Figure 8. Distribution of NHEJ markers at different stages of prophase-I by recovery time after irradiation. SYCP3 (green) and XRCC4 (red) in late prophase-I spermatocytes. (A-C) Control. XRCC4 is absent up to mid pachytene (A). At late pachytene (B), a faint signal is observed in the nucleus, which becomes more intense at diplotene (C). The signal appears more concentrated on the sex chromosomes (XY). (D-F) 1 hour, (G-I) 24 hours and (J-L) 72 hours after irradiation. The localization pattern of XRCC4 at each stage is almost identical. Foci do not form at any stage or recovery time.

Figure 9. Pattern of 53BP1 at different stages of prophase-I by recovery time after irradiation. SYCP3 (red), γH2AX (blue) and 53BP1 (green). (A-C) Control. 53BP1 is first detected at mid pachytene (A) around the sex chromosomes and is maintained during late pachytene (B) and diplotene (C). During diplotene, the signal weakens, becoming no longer detectable by the end of this stage. The 53BP1 signal co-localizes with γH2AX around the sex chromosomes, X and Y. (D-F) 1 hour of recovery. From mid pachytene (D) onwards, a large number of 53BP1 foci appear on the autosomes as diffuse clouds. The 53BP signal is similarly maintained in late pachytene (E) and diplotene (F) spermatocytes, although foci become smaller as prophase-I progresses. Arrows indicate the bivalents shown in details. These 53BP1 signals largely coincide those of γH2AX (red arrowheads), although γH2AX foci without 53BP1 are also present (blue arrowheads) (see detail in E). (G-I) 24 hours of recovery. A noticeable decrease in the number of 53BP1 and γH2AX foci occurs relative to the 1-hour time point. In some cases, these foci coincide with those of γH2AX (red arrowhead in left detail in H) and in others they do not (blue arrowhead right detail in H). (J-L) 72 hours of recovery. The number and distribution of 53BP1 and γH2AX foci are similar to those at 24 hours. The presence of two interstitial bridges between autosomal bivalents (arrows) can be more clearly seen in the enlarged details in (J). γH2AX is observed on one of the bridges (right), whereas both γH2AX and 53BP1

1132 are co-localized on the other (left). (M) Dotplot of the number of 53BP1 foci in spermatocytes grouped by
1133 recovery times. Three substages were considered (MP: mid pachytene; LP: late pachytene; ED: early
1134 diplotene). Increased numbers of foci are evident 1 hour after irradiation. ANOVA analysis showed
1135 statistical differences at this time between the three stages analyzed ($p \leq 0.0001$). Tukey's multiple
1136 comparisons test for individual comparisons between different stages showed no statistical differences
1137 between LP and ED cells. A reduction is observed in the number of foci in cells at all stages 24 hours after
1138 irradiation. An analogous situation is found 72 hours after irradiation. (N) Dotplot of the number of 53BP1
1139 foci in spermatocytes grouped by stage. Cells at all stages return to control levels 72 hours after irradiation.
1140 ns: non-significant; *: $p \leq 0.05$; **: $p \leq 0.01$; ***: $p \leq 0.001$; ****: $p \leq 0.0001$.

1141

1142 **Figure 10. Model for the transition of the DNA damage response during meiosis.** The early (meiotic)
1143 response works from early leptotene up to mid pachytene and is characterized by the action of HR
1144 mechanisms. This is the default pathway, likely due to the programmed resection of DNA upon SPO11
1145 removal, which would hamper the action of NHEJ mechanisms. The meiotic response involves broad
1146 phosphorylation of γH2AX in the nucleus, likely in association with changes in chromatin organization,
1147 epigenetic modifications and transcriptional silencing, characteristic features of spermatocytes at these
1148 stages. DMC1 and RAD51 work together during this early response. DMC1 is removed first, leaving only
1149 RAD51 at the last stages of this response, which may affect interhomolog bias in the repair of DSBs.
1150 Induction of additional exogenous DSBs (but also potentially spontaneous, SPO11-independent ones)
1151 triggers an identical meiotic response, marked by the massive γH2AX localization throughout the nucleus
1152 and the increase of DMC1 and RAD51 in cells at all stages up to mid pachytene. Although γH2AX is quickly
1153 removed, many unresolved DNA damage intermediates accumulate even after long periods of recovery,
1154 indicating that this mechanism is not completely efficient. The dual late response very much resembles

the response of somatic cells, including the appearance of discrete γH2AX foci. NHEJ is the first mechanism activated in this late somatic-like response, triggered soon after induction of DSBs from mid pachytene onwards. Some factors, like 53BP1, may already be present and localized on the sex chromosomes, with others (Ku70, XRCC4) appearing by default during late pachytene. This mechanism can quickly respond to DNA damage and, under normal conditions, likely resolve most, if not all, endogenously generated DSBs. However, after the induction of an exceeding number of DSBs, the initial NHEJ response is replaced by a HR one, involving only RAD51. Although this somatic-like response is less efficient in removing γH2AX than the early meiotic response, its overall repair efficiency is probably similar. Indeed, lower accumulation of unresolved intermediates is observed for this late response after long periods of recovery. The transition between these two DNA damage responses clearly occurs during mid pachytene, when the meiotic response is no longer inducible and the somatic-like one becomes available. This transistion indicates a possible physiological shift in meiotic cells as they prepare for further stages of first meiotic division and, more relevantly, chromosome segregation.

Supplementary information

S1 Figure. Estimated length of meiotic stages, based on previous reports by Oakberg [48] and Ashley and coworkers [47].

S2 Figure. Apoptosis induction after irradiation. TUNEL (green) and DAPI (blue). (A-C) Section of a seminiferous tubule 24 hours after treatment. Apoptotic cells are found in both the basal (arrows) and interstitial (arrowheads) strata of the seminiferous epithelium. (D-F) Section of a seminiferous tubule 72 hours after treatment showing apoptotic cells at metaphase or anaphase. (G-I) Detail of apoptotic metaphase and anaphase cells 72 hours after irradiation. Note the presence of chromatin bridges between cell poles in the anaphase cell (arrow in G). (J). Quantitative distribution of apoptotic cells. Total number of apoptotic cells were recorded in 300 seminiferous tubules. Peak apoptosis is observed 24 after irradiation with 58.6% of tubules showing at least one apoptotic cell. At this time, spermatogonia are the most affected population, followed by spermatocytes and cells undergoing division. After 72 hours of recovery, the total number of apoptotic cells decreases with only 27.6% of tubules showing apoptotic cells. At this recovery time, the majority of cells undergoing apoptosis are at metaphase or anaphase.

S3 Table. Quantitative data for all proteins analyzed and chromosomal bridges organized by cell stage and recovery time.

S4 Figure. DMC1 localization in SPO11 knockout mice. (A-C) SYCP3 (green) and (A'-C') DMC1 (red) at early leptotene (A, A'), mid leptotene (B, B') and zygotene-like (C, C'). No specific signal of DMC1 is detected at any of the stages analyzed.

S5 Figure. Quantitative analysis of DMC1 dynamics during early prophase-I. Cell progression during prophase-I and duration of each stage is represented in the series of images at the top. Distribution of DMC1 foci are arranged according to the recovery time after irradiation and the putative stages that cells

should have reached at that time, provided that meiotic progression was not affected by the treatment. We arranged four cell populations: early leptotene, mid-late leptotene, early-mid zygotene and late zygotene. For each case, irradiated cells were compared with their respective control counterparts and statistical differences indicated (ANOVA and Tukey's multiple comparisons test). Only cells that advanced to mid pachytene during the recovery time, i.e., those that were irradiated at early or late zygotene, show control levels of DMC1 after 72 hours of recovery. This is mostly due to the fact that DMC1 is not inducible at this stage and/or the programmed displacement of DMC1 from the chromosomes, regardless of whether repair had been completed or not. EL: early leptotene; LL: mid-late leptotene; EZ: early-mid zygotene; LZ: late zygotene; EP: early pachytene; MP: mid pachytene; ns: non-significant; *: p≤0.05; **: p≤0.01; ***: p≤0.001; ****: p≤0.0001.

S6 Figure. **Localization of DMC1 and RAD51 in control spermatocytes**. SYCP3 (blue), DMC1 (green) and RAD51 (red). Merge of the (A-F) SYCP3 and DMC1 channels, (A'-E') SYCP3 and RAD51 channels and (A''-F'') SYCP3, DMC1 and RAD51 channels. DMC1 and RAD51 are largely co-localized in foci observed from early leptotene to mid pachytene (A-D). However, DMC1 and RAD51 signal on these foci are usually not identical in size or shape. Moreover, there are some instances in which either of the two proteins seem to form single foci. At mid-late pachytene (E-E''), DMC1 is no longer present on the chromosomes, but RAD51 is still abundantly observed on both autosomes and sex chromosomes (X and Y). By late pachytene (F-F''), neither DMC1 nor RAD51 are observed.

S7 Figure. **Localization of DMC1 and RAD51 at different stages of prophase-I by different recovery time after irradiation**. SYCP3 (blue), DMC1 (green) and RAD51 (red). (A-F) Control. The cells shown in A-D are the same as those shown in S6 Figure. (G-L) 1 hour after irradiation. As shown in Figures 4 and 6, both DMC1 and RAD51 become more abundant after irradiation with both proteins being present in the same foci in most cases; however, the overlap in signals is not identical in many instances as the sizes and shapes

1215 of foci of the individual proteins differ. From late pachytene onwards, only RAD51 foci are detectable. (M-
1216 R) An analogous result is found 24 after irradiation. Filaments containing both DMC1 and RAD are observed
1217 in some spermatocytes (arrows in M).

1218 **S8 Figure**. **Localization of XRCC4 in testicular sections**. γH2AX (green), XRCC4 (red) and DAPI (blue) in
1219 seminiferous tubules at equivalent developmental stages. (A-D) Control. Basal layers of spermatocytes,
1220 corresponding to leptotene and zygotene, are broadly stained with γH2AX and devoid of XRCC4.
1221 Spermatocytes in the interstitial strata of the epithelium show an inverse labeling pattern, with abundant
1222 XRCC4 and nearly no γH2AX staining. (E-H). 1 hour after irradiation. Cells showing broad γH2AX labeling in
1223 the basal strata are again devoid of XRCC4. In contrast, spermatocytes stained with XRCC4 now also have
1224 an abundance of γH2AX localized foci, corresponding to the late γH2AX response. No noticeable increase
1225 in the intensity of XRCC4 labeling is observed. (I-L) 24 hours and (M-P) 72 hours after irradiation. γH2AX
1226 tend to return to control levels. No variation of XRCC4 labeling is observed after longer periods of recovery.

1227

1228

FIGURE 1

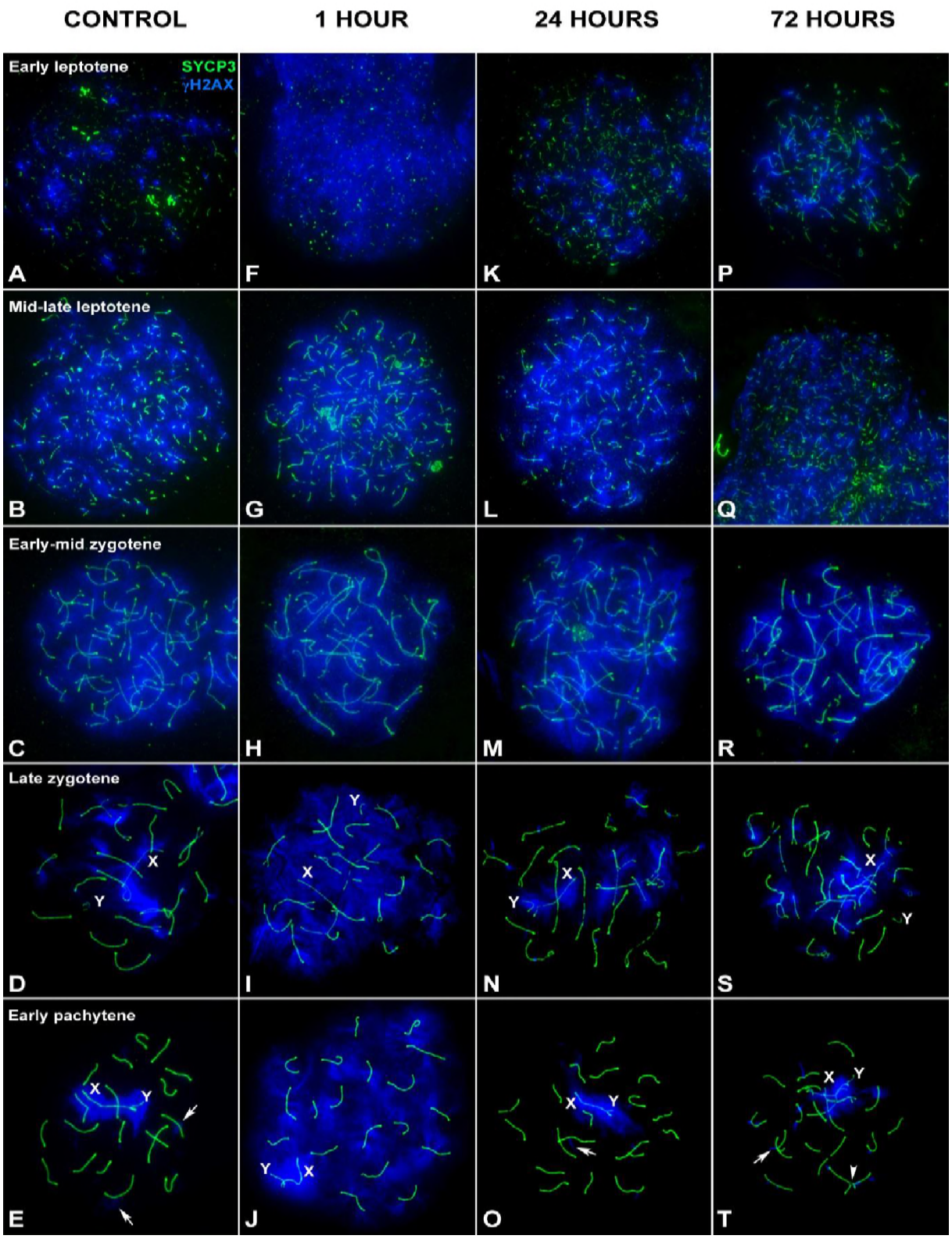

1229

FIGURE 2

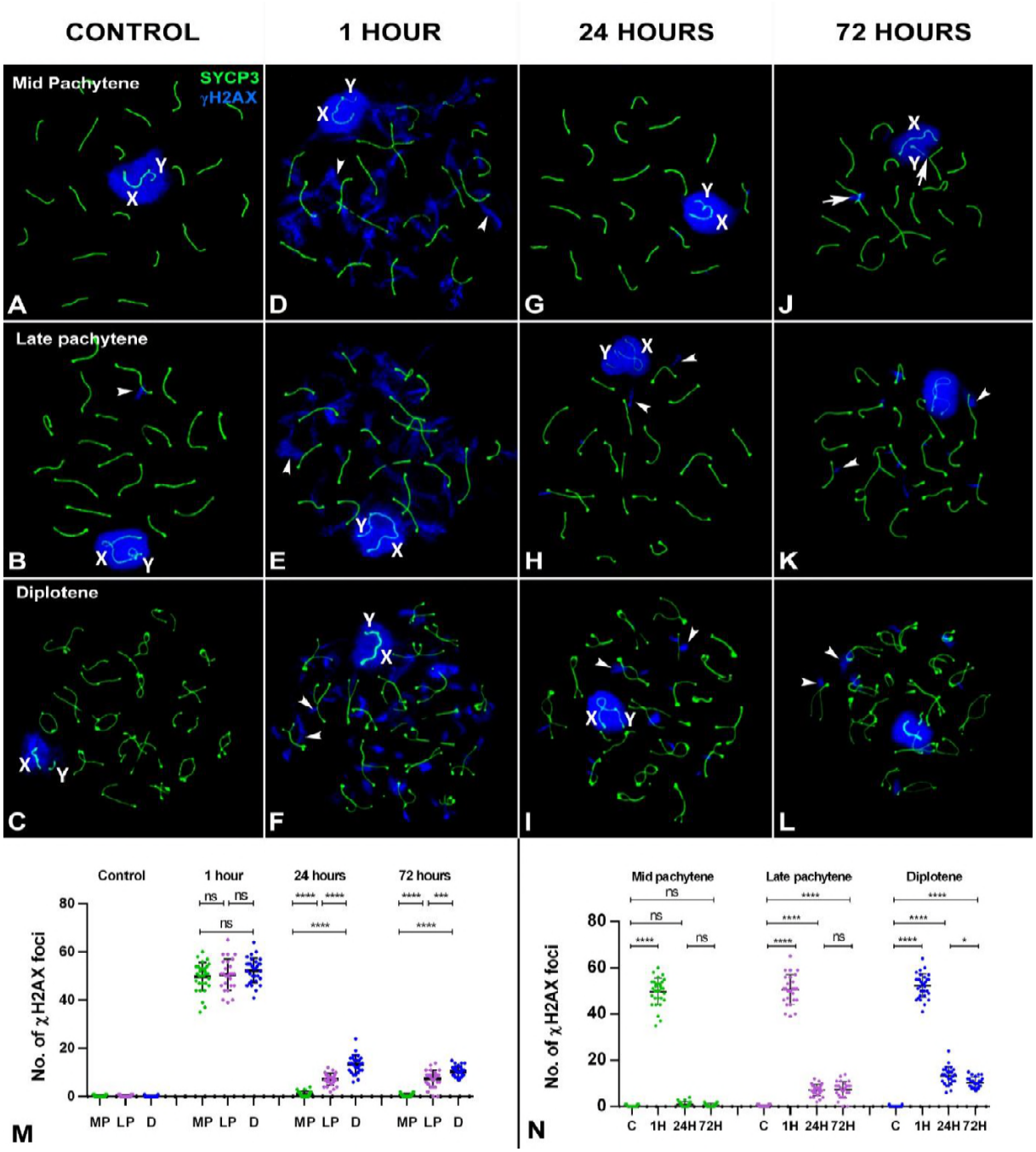

1233

FIGURE 3

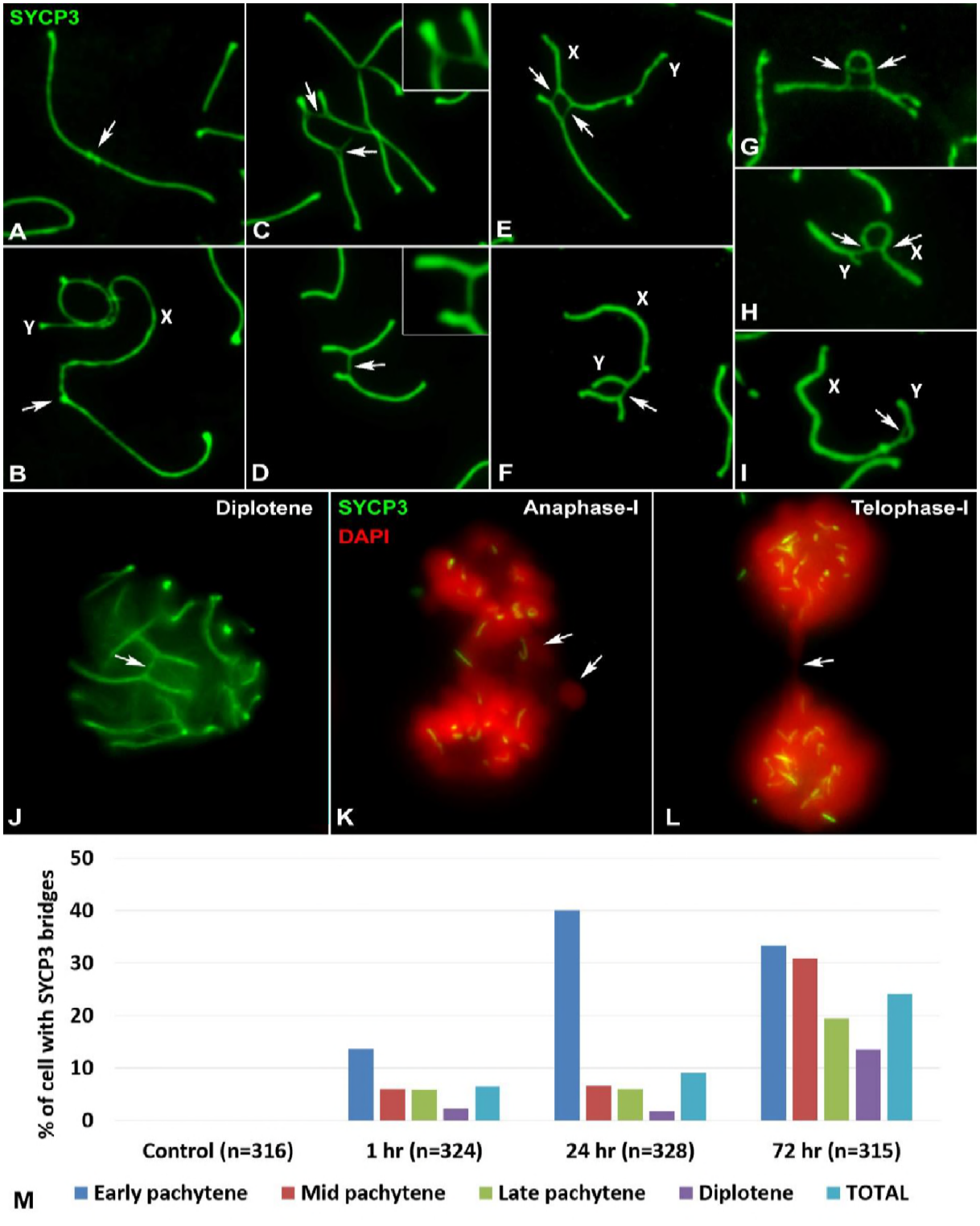

1234

1235

1236

FIGURE 4

1237

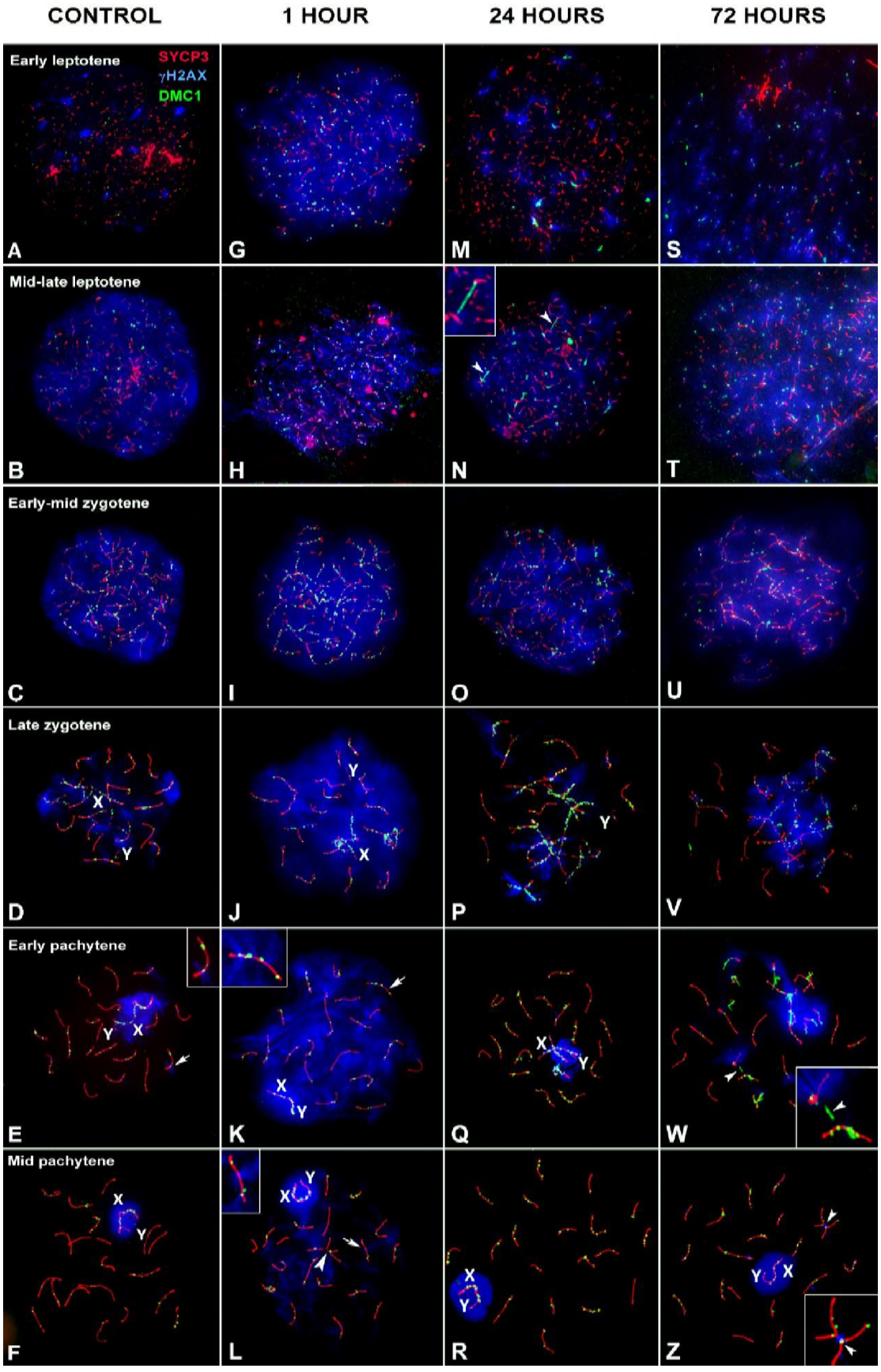

1238

FIGURE 5

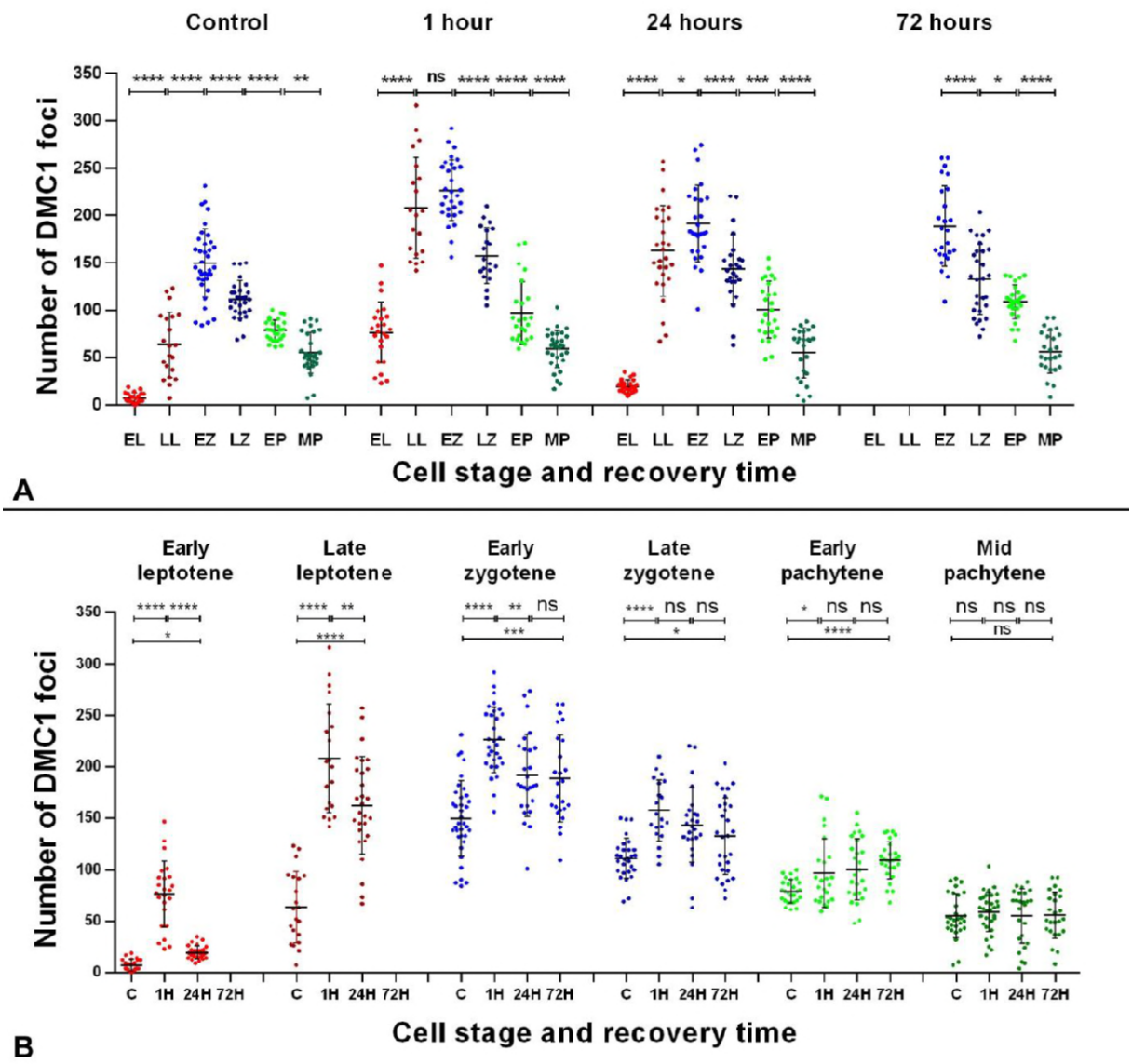

1239

1240

1241

FIGURE 6

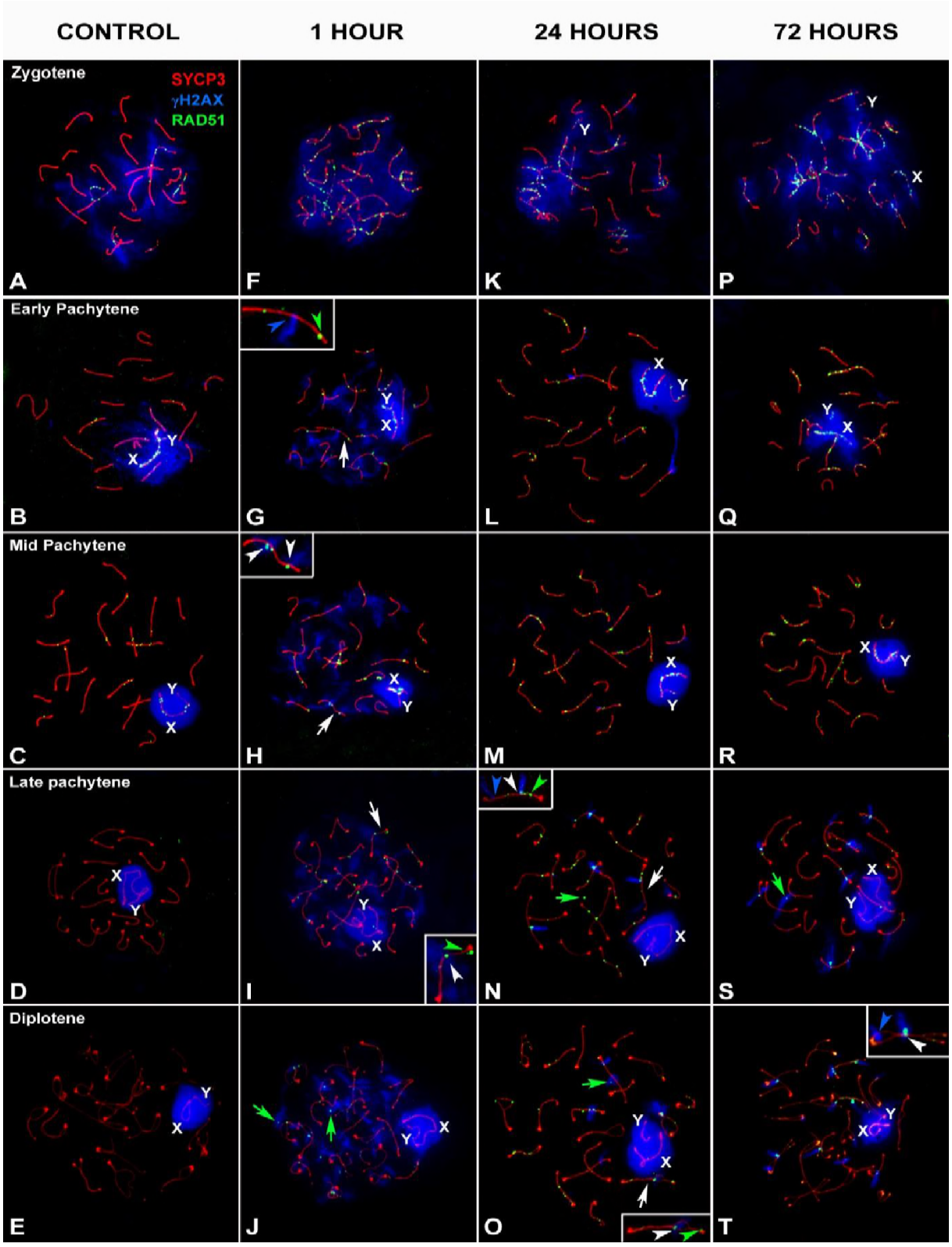

1242

1243

FIGURE 7

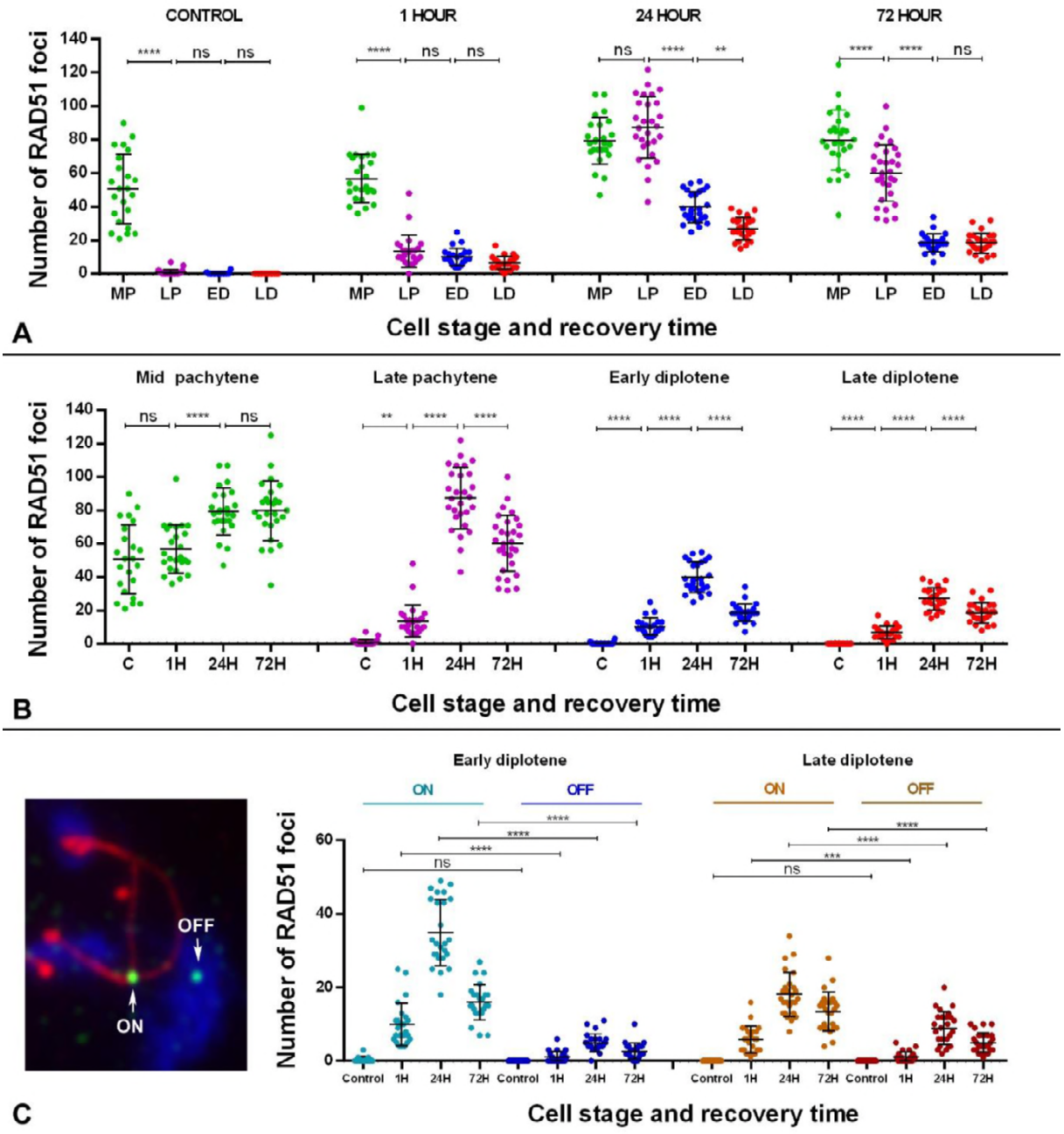

1244

1245

1246

FIGURE 8

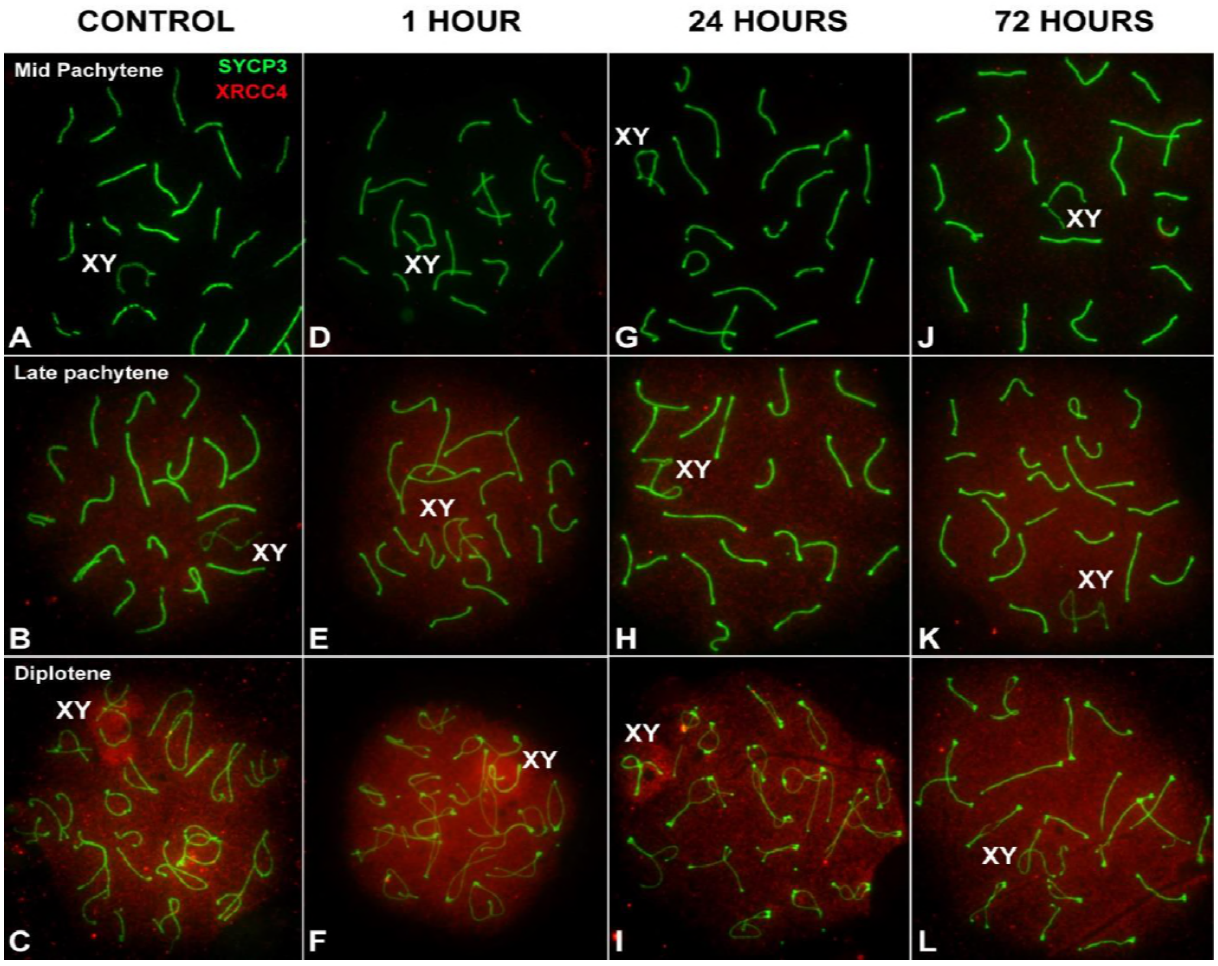

1247

1248

1249

FIGURE 9

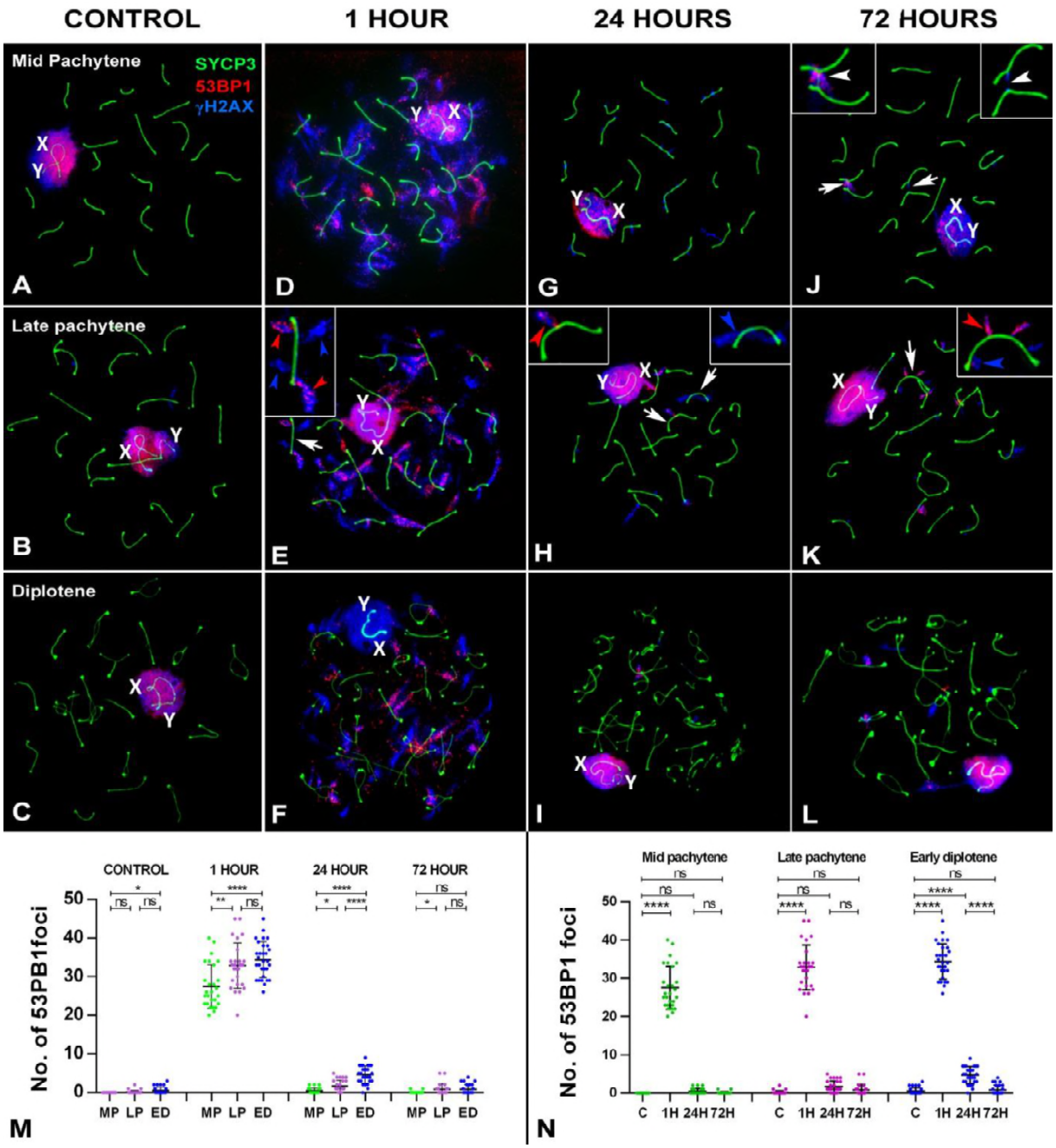

1250

1251

1252

FIGURE 10

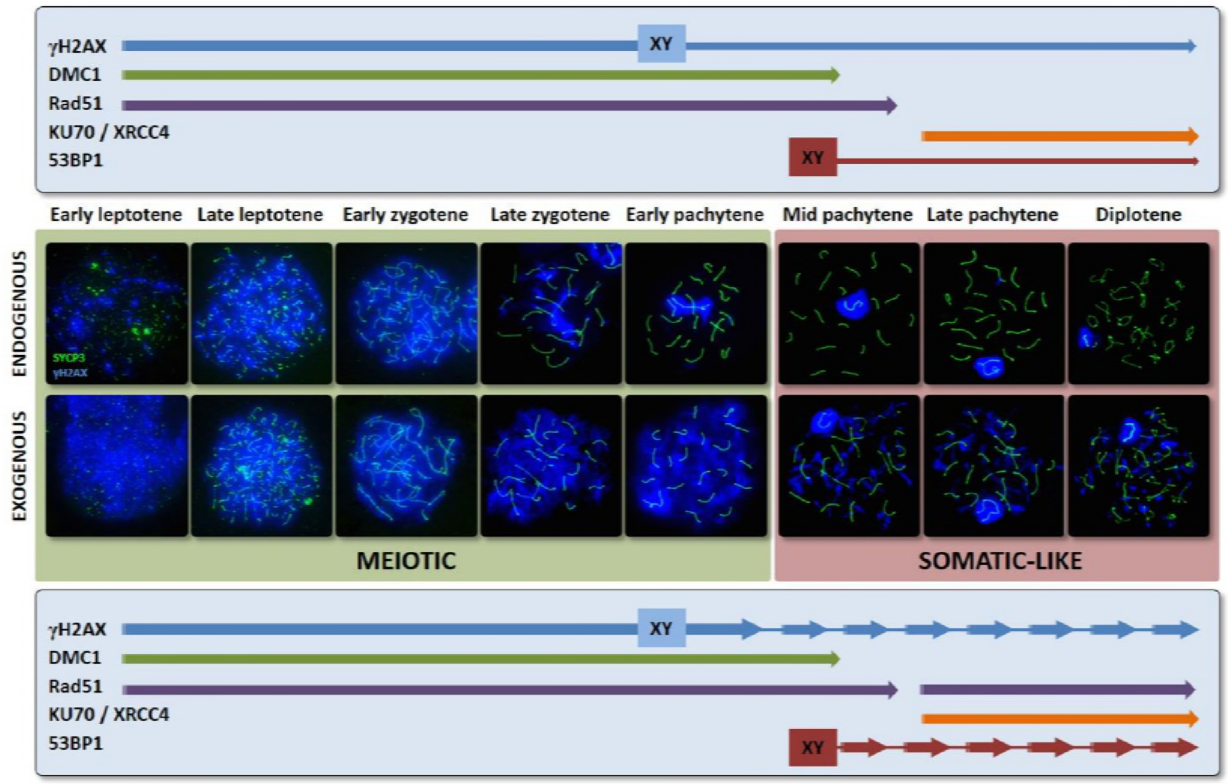

1253

1254

1255

S1 FIGURE

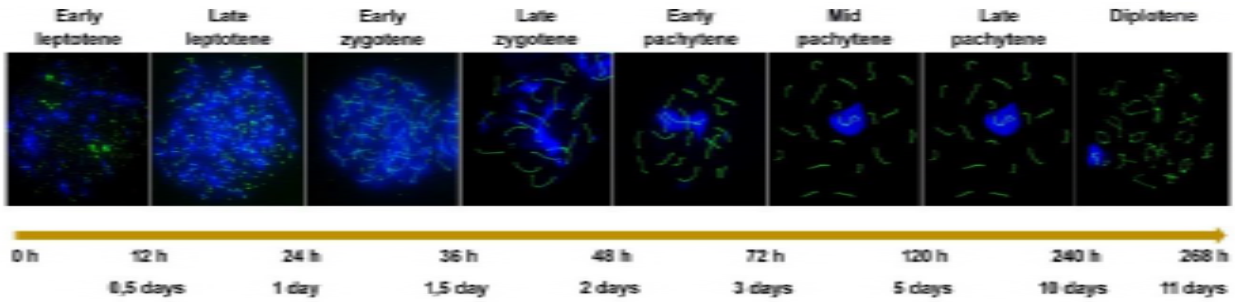

1256

1257

1258

1259

S2 FIGURE

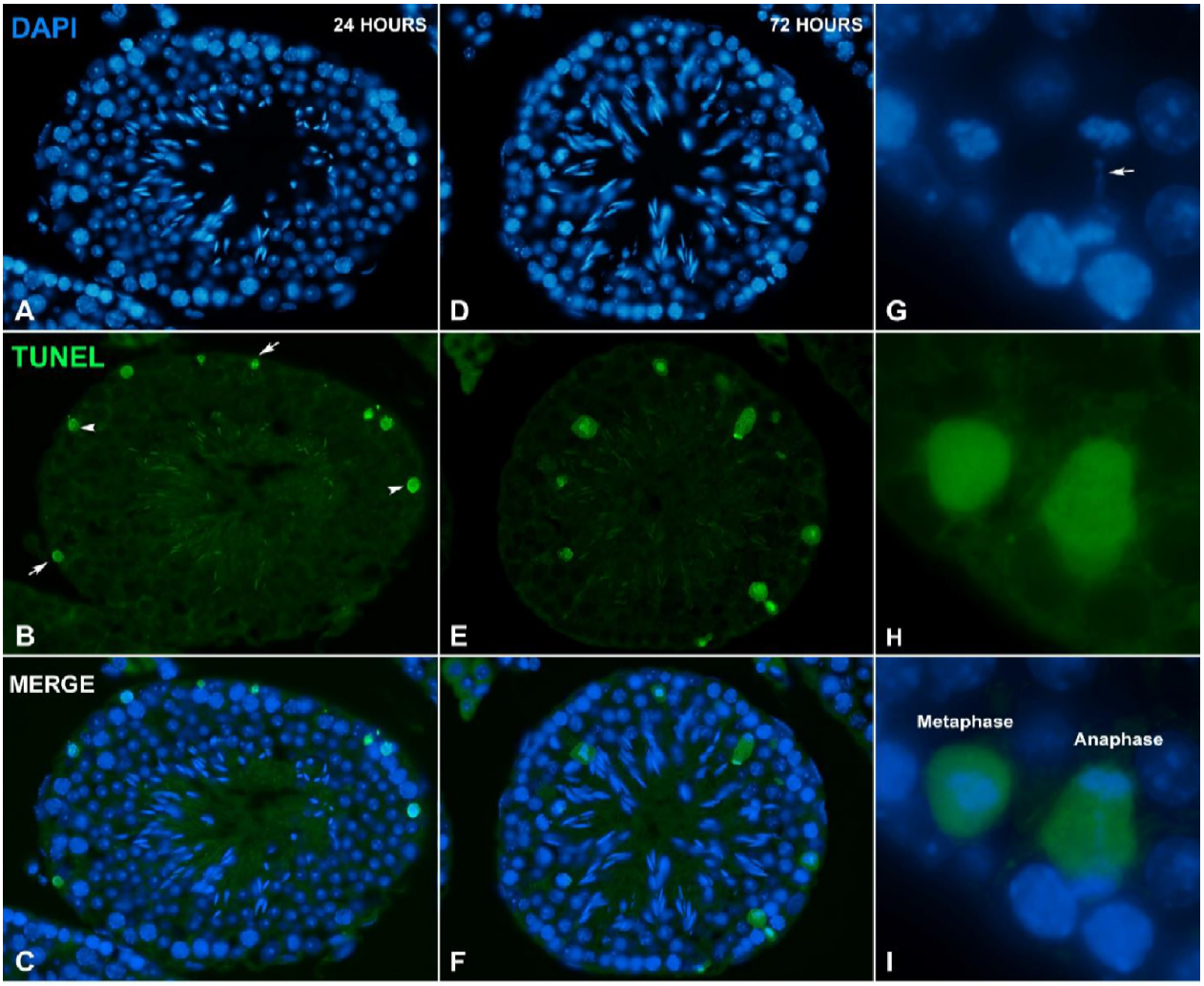

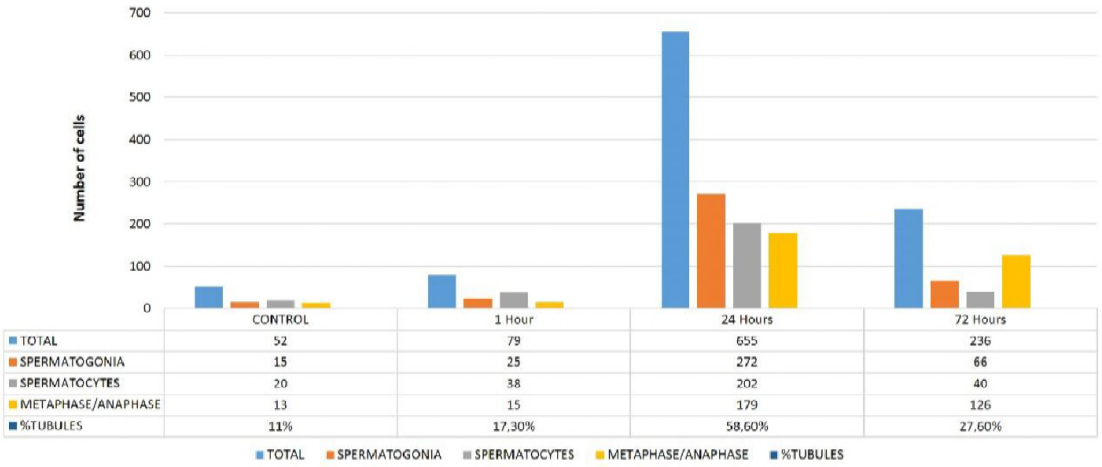

J

1260

1261

1262

S3 TABLE

γH2AX	Mid pachytene			Late Pachytene			Early Diplotene		
	Mean	SD	n	Mean	SD	n	Mean	SD	n
CONTROL	0.23	0.43	25	0.31	0.47	25	0.08	0.27	25
1 HOUR	50.66	4.72	29	51.46	5.89	25	52.96	4.61	29
24 HOURS	1	1.17	26	7.15	2.38	26	13.31	3.89	26
72 HOURS	0.54	0.71	26	7.35	3.59	26	10.38	2.33	26

1263

BRIDGES	Early pachytene		Mid pachytene		Late Pachytene		Early Diplotene		TOTAL	
	%	n	%	n	%	n	%	n	%	n
CONTROL	0	48	0	101	0	110	0	57	0	316
1 HOUR	13.64	44	5.98	117	5.93	118	2.22	45	6.48	324
24 HOURS	40.00	35	6.67	120	5.98	117	1.79	56	9.15	328
72 HOURS	33.33	21	30.89	123	19.40	134	13.51	37	24.13	315

1264

DMC1	Early Leptotene			Mid-late Leptotene			Early-mi Zygotene			Late Zygotene			Early Pachytene			Mid Pachytene		
	Mean	SD	n	Mean	SD	n	Mean	SD	n	Mean	SD	n	Mean	SD	n	Mean	SD	n
CONTROL	7.04	5.39	24	63.62	34.49	21	149.75	36.41	36	111.10	19.74	29	78.89	11.08	27	55.00	21.21	29
1 HOUR	76.08	32.15	24	208.25	53.11	20	226.57	32.06	30	157.50	29.62	20	96.79	33.14	24	58.87	19.49	31
24 HOUR	19.48	6.45	27	162.68	47.62	28	191.70	40.12	27	143.36	36.43	25	100.50	29.76	26	54.96	26.56	25
72 HOUR							188.60	42.45	25	132.62	33.07	29	108.96	18.01	27	55.88	22.51	25

1265

RAD51	Mid pachytene			Late Pachytene			Early Diplotene			Late Diplotene		
	Mean	SD	n	Mean	SD	n	Mean	SD	n	Mean	SD	n
CONTROL	50.61	20.76	23	0.85	1.66	25	0.23	0.65	25	0	0	26
1 HOUR	56.80	14.42	27	16.62	18.06	28	11.04	6.60	24	6.64	3.82	30
24 HOURS	79.36	14.07	26	87.36	18.51	23	41.08	12.18	25	27.04	4.53	25
72 HOURS	79.88	17.95	25	60.10	16.92	25	18.64	5.44	26	18.42	6.00	26

1266

RAD51	Early diplotene ON			Early diplotene OFF			Late Diplotene ON			Late Diplotene OFF		
	Mean	SD	n	Mean	SD	n	Mean	SD	n	Mean	SD	n
CONTROL	0.23	0.65	25	0	0	25	0	0	26	0	0	26
1 HOUR	10.00	5.78	24	1.04	1.51	24	5.83	3.64	24	1.08	1.41	24
24 HOURS	36.12	8.96	25	4.96	2.46	25	18.12	6.05	26	8.92	4.53	26
72 HOURS	15.96	4.83	26	2.68	2.17	26	13.42	5.30	26	5.00	2.70	26

1267

53BP1	Mid pachytene			Late Pachytene			Early Diplotene		
	Mean	SD	n	Mean	SD	n	Mean	SD	n
CONTROL	0.00	0.00	25	0.16	0.47	25	0.50	0.91	26
1 HOUR	27.48	5.62	27	32.85	5.89	27	34.33	4.66	30
24 HOURS	0.48	0.71	25	1.63	1.55	27	4.63	2.22	27
72 HOURS	0.08	0.28	25	0.84	1.40	26	0.81	1.27	25

1268

1269

1270

S4 FIGURE

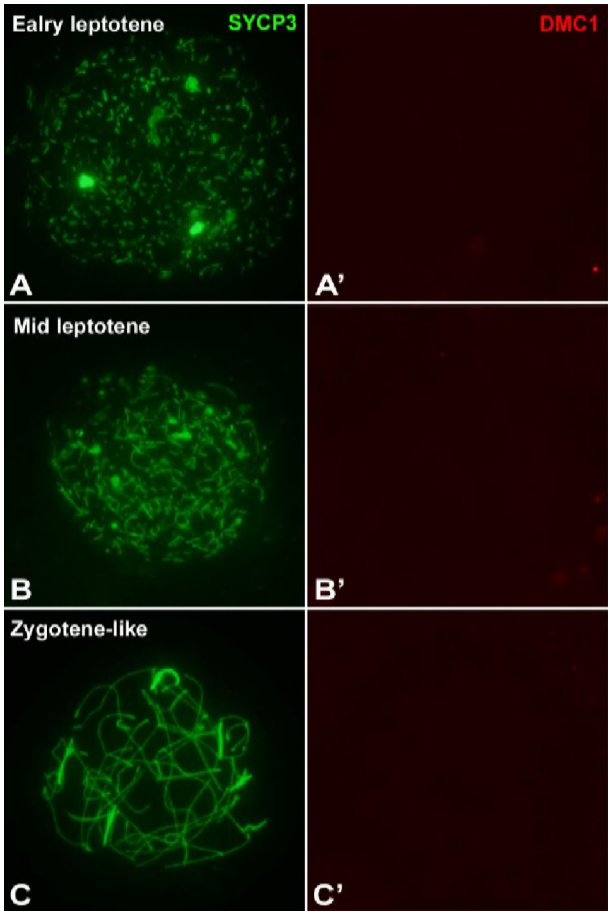

1271

1272

1273

S5 FIGURE

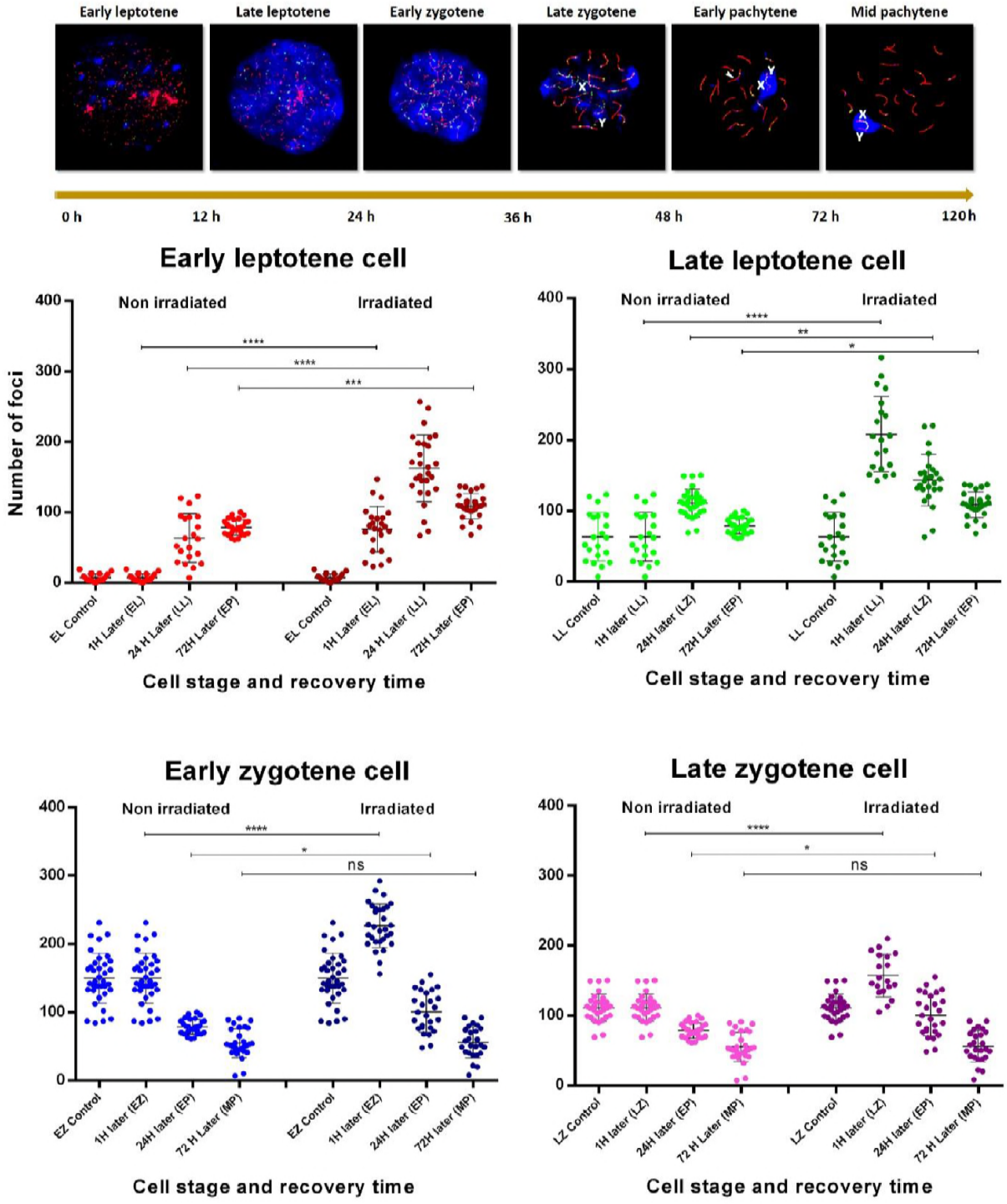

1274

1275

1276

S6 FIGURE

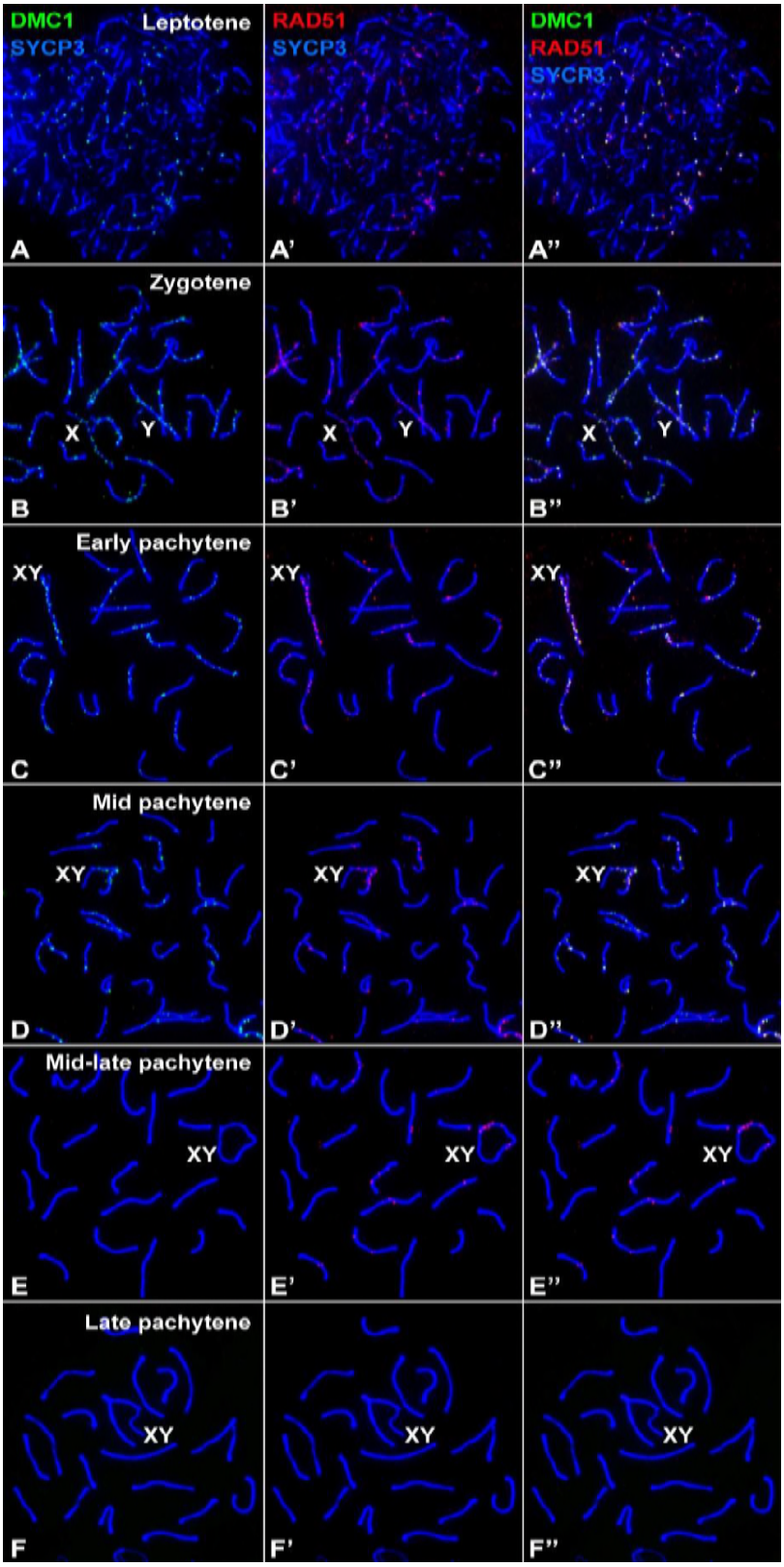

1277

1278

S7 FIGURE

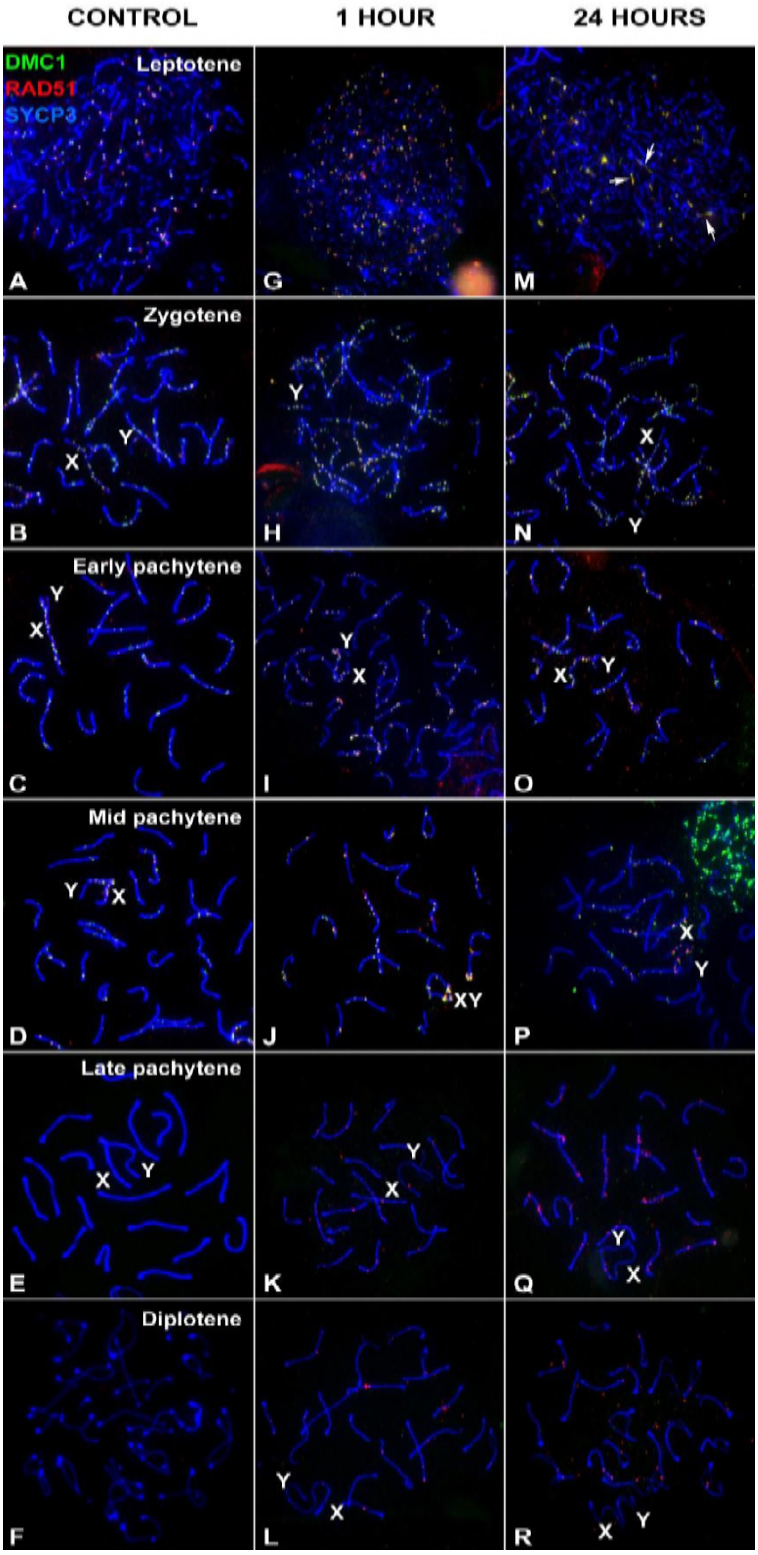

1279

1280 **S8 FIGURE**

1281

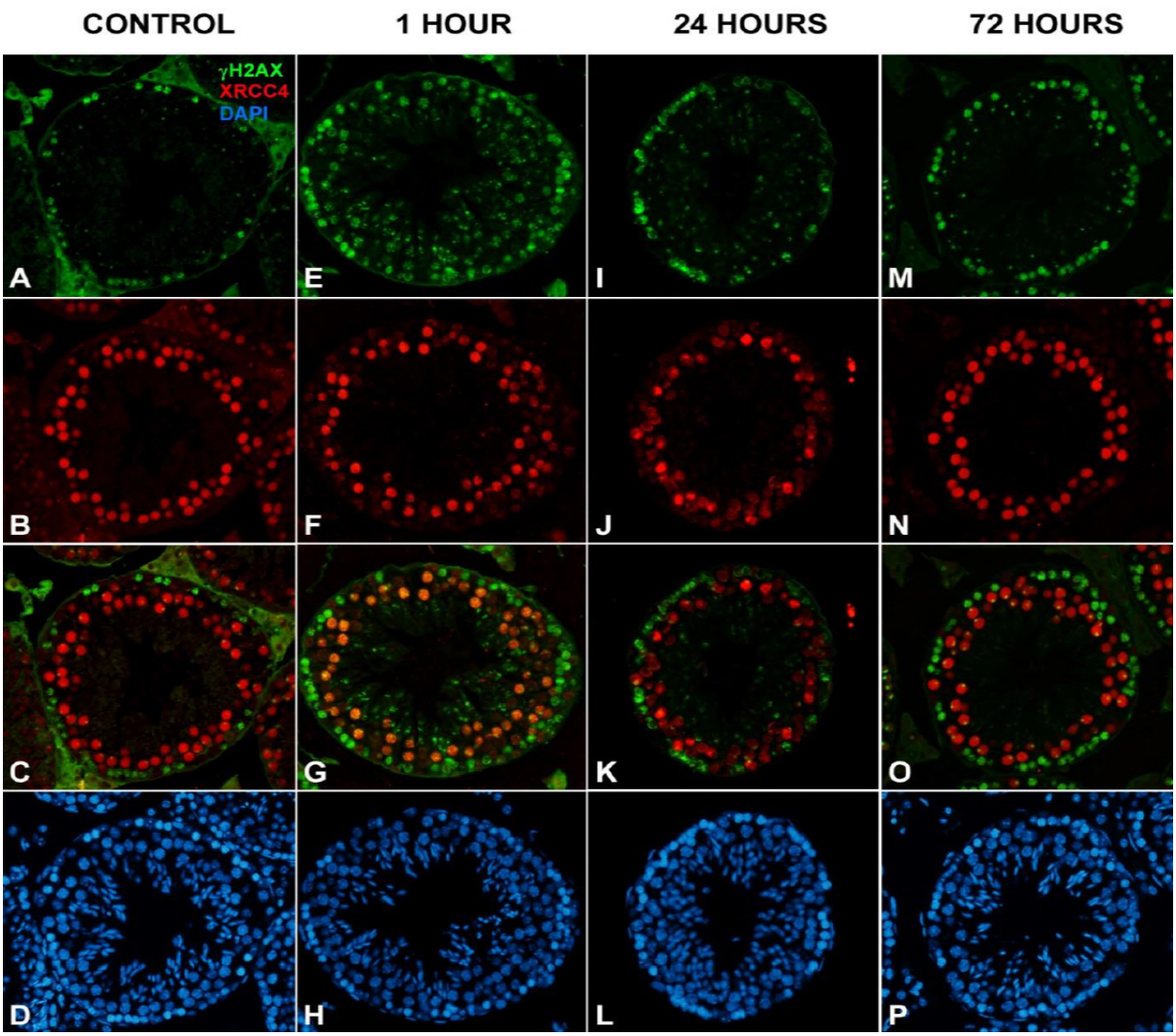

1282